https://doi.org/10.5194/egusphere-2026-5168
Preprint. Discussion started: 11 September 2026

Tidal forcing causes bi-decadal variability in dissolved oxygen: clarification with a causal discovery method

Benedict Blackledge[1], Oliver Andrews[2], Rory Bingham[3], Urmi Ninad[4], and J. A. Mattias Green[5]

[1]Department of Earth, Ocean and Ecological Sciences, University of Liverpool, Liverpool, UK
[2]Department of Environment and Geography, University of York, York, UK
[3]School of Geographical Sciences, University of Bristol, Bristol, UK
[4]Department of Computer Science, University of Potsdam, Potsdam, Germany
[5]School of Ocean Sciences, Bangor University, Menai Bridge, UK

Correspondence: Benedict Blackledge (b.blackledge@liverpool.ac.uk)

Abstract. Identifying the mechanisms behind the trends and variability in observations of ocean oxygen concentration (O_2) is key to understanding long-term ocean deoxygenation. But this task remains challenging, as observations contain persistent signals from interacting physical and biogeochemical processes. Here we apply the time series causal discovery method, PCMCI, to a dataset of O_2 from the Oyashio region in the North West Pacific to test whether a causal relationship from the nodal cycle in the tidal forcing on to the O_2 exists. We identify causal links from the tidal index to O_2 and apparent oxygen utilisation (AOU), concentrated between approximately $27.35\sigma_\theta$ and $26.75\sigma_\theta$, with a characteristic lag of approximately two years. The tidal effect on O_2 is only present at densities greater than the density of the late-winter mixed layer (the base of the mixed layer), with a maximum causal link at around $27.1\sigma_\theta$. Little evidence is found for a causal relationship with the O_2 solubility. Compared to lagged correlation, PCMCI detects a reduced strength and density distribution of the tidal effect and removes much of the lag structure while retaining the characteristic 2 year lag. The density and lag structure are consistent with transport and enhanced tidal mixing from within the Sea of Okhotsk system and the Kurils, but we cannot identify a geographical location or the complete physical pathway of the causal effect with the existing observations. It may be the case that several causal models are compatible with the existing data. These results show the promise of causal inference and discovery methods within oceanographic problems.

1 Introduction

Across the Pacific, continuously occupied oceanographic stations have revealed that the marine dissolved oxygen concentration (O_2) varies considerably over monthly (Whitney et al., 2007), interannual (Stramma et al., 2020) and decadal (Sasano et al., 2015, 2018) time scales. This variance is in addition to the persistent deoxygenation signal that is forced by global climate change (Oschlies et al., 2018), a signal that is now observed in nearly all multi-year time-series and aggregated observations distributed through the global ocean (Schmidtko et al., 2017; Ito et al., 2017; Stramma and Schmidtko, 2019). A clear goal of research investigating ocean O_2 dynamics then, is to identify the physical and biogeochemical causal processes which determine the variability in O_2 and its secular changes. Unfortunately, the complexity of ocean-biogeochemistry-atmosphere

https://doi.org/10.5194/egusphere-2026-5168
Preprint. Discussion started: 11 September 2026

interactions and the wide range of time-scales over which they occur within the oceans, can render the underlying causes of O_2 trends and variability opaque. For example, the solubility of O_2 in sea water (O_2^{sat}) is a function of temperature and salinity (Garcia and Gordon, 1992), and gas exchange forms a crucial part of the O_2 budget. Air-sea interactions are "fast", so O_2 within the surface mixed layer is generally equilibrated with the atmosphere. In contrast, the interior O_2 is determined by the ocean's dynamics, mixing and advection, but this redistribution is comparatively slow – taking place over months and years. Simultaneously the ocean integrates the production of O_2 by phytoplankton and crucially its consumption by respiration, moving O_2 away from O_2^{sat}. Once a water parcel sinks below the surface mixed layer, ventilating the ocean interior, apparent oxygen utilisation (AOU) accumulates from the respiration of oxygen and the mixing of water masses with different O_2 concentrations (Jutras et al., 2025). While these exact process histories are inaccessible outside of models constructed for that purpose, observational campaigns and modelling indicate that the ocean dynamics within the sea of Okhotsk (SO) and the Kurils (Figure 1a) is essential for the ventilation of the Pacific interior (Mensah et al., 2024). Distinguishing the relative importance of different processes and their interactions however, has remained a challenge.

Recent work has focussed on using Earth System Models (ESMs) to quantify forced changes and natural variability in O_2 (Long et al., 2016). These models have provided us with considerable explanatory power in terms of detecting external forcing in the observed global deoxygenation signal (Andrews et al., 2013) and the dynamical response of the ocean to a changing climate (Palter and Trossman, 2018). These are questions which could not be addressed experimentally without the use of dynamical models. However, it is well known that even state-of-the-art ESMs underestimate both the variability in O_2 and regional to global deoxygenation trends (Oschlies et al., 2018). While these discrepancies will likely depend on the specific model used, ESM simulations compared directly with time series observations often underestimate the interannual variability in the observed O_2 concentration by a factor of 2 to 3 (Long et al., 2016). The reasons for these limitations have been widely discussed elsewhere (Oschlies et al., 2018), but many of these factors can be broadly categorised as systematic issues in the ESM architecture, e.g., imperfect parameterisations of ocean mixing (Gnanadesikan et al., 2012; Bahl et al., 2019; Lévy et al., 2022) or uncertainties in the representation of ecosystem processes (Rohr et al., 2023). Finally, a key assumption is that the set of processes comprising the model (an ESM or any other form of *parametric* model) are sufficient to explain the dynamics of the observations it is compared to (Flato, 2011). The question then is, how do we identify processes responsible for observed O_2 variability in such a complex system without relying on a predefined parametric model?

Other disciplines facing comparably challenging questions have drawn on the field of causal inference (Camps-Valls et al., 2023). As the name implies, these are methods designed to identify and quantify cause $\rightarrow$ effect relationships between variables, rather than merely identifying statistical associations within the data. It is important to highlight for the reader unfamiliar with causal inference that this is a broad family of methods built on a now well-developed body of theory (Pearl, 2009b). These methods share some general, yet important, attributes. The researcher is forced to consider their data as being an end product of some unknown or partially-known (but desired) data generating process, commonly represented as a causal graph. Alternatively, the researcher can "discover" a causal graph from the data (causal discovery), using causal inference theory and limited sets of assumptions about their data and the system it represents (Runge et al., 2019a; Camps-Valls et al., 2023). By specifying a causal model, the researcher is forced to consider the effects of confounding variables (a common cause between

https://doi.org/10.5194/egusphere-2026-5168
Preprint. Discussion started: 11 September 2026

two or more variables) and latent (unobserved) variables in the representation of the data generating process. In many cases, it might not be possible to identify a causal model given the data at hand, a critical distinction with traditional statistical modelling. With a causal model tested and in hand, powerful techniques such as causal effect estimation and counterfactual analysis can then be performed (Pearl, 2009b; Hannart et al., 2016).

Observational datasets can only partially represent complex marine ecosystems, yet we still require cause → effect knowledge of the constituent processes that generated our observations. Correctly identifying the relevant variables and their interactions is essential for estimating how marine ecosystems will change when one or more causal processes are perturbed under a changing climate. A specific example of a potential causal process of O_2 is tidal mixing. This is mixing resulting from the ocean's response to the Lunisolar gravitational forcing (further detail is given in Section 1.2) (Pugh, 2014). Such forcing is close to being an ideal potential cause, because the principle mechanism neatly fulfils the definition of exogeneity (Pearl, 2009b) - a variable determined by processes outside of the system under analysis. The only comparable forcing processes in oceanography are solar forcing, rotation and arguably the radiative forcing of the atmosphere (Hannart and Naveau, 2018). In this study we intend to build on previous work associating tidal forcing with variability in oceanic O_2 (Sasano et al., 2018). We apply a graphical causal discovery method to a historical O_2 time series from the Oyashio region (Figure 1a), which we describe in below Section 1.1. The causal discovery method is outlined in Section 2.2. Details of the relevant ocean and tidal dynamics are given in Section 1.2.

1.1 Oxygen variability in the Oyashio region of the North Pacific

The high density of oceanographic observations in the North Western Pacific permits a more detailed investigation into the origins of O_2 variability than many other ocean regions. The Oyashio marine ecosystem region, for example, to the East of Hokkaido (Figure 1a), has been regularly sampled since the 1930s (Sasano et al., 2018), yielding one of the longest continuous O_2 records anywhere in the oceans (Figure 1b). There are two key properties of this time series, shown in Figure 1b - the deoxygenation trend and the presence of "bidecadal" oscillations around the deoxygenation trend (Sasano et al., 2018). The presence of both has raised a number of questions over their driving processes. For example, it was suggested that the deoxygenation signal originates from a reduced vertical O_2 exchange from the surface (Mecking et al., 2008). Yet, as the deoxygenation trend exists at densities greater than the maximum outcropping density (Ono et al., 2001), this is unlikely to be the sole explanation (Sasano et al., 2018). The oscillations around the linear decrease in dissolved oxygen (Figure 1c) have been attributed to the nodal variation in tidal mixing (Sasano et al., 2018). The period of the oscillations, estimated with various methods, is reported as being between 18.5 and 20 years (Ono et al., 2001; Osafune and Yasuda, 2006; Sasano et al., 2018). In addition to O_2, bidecadal oscillations have been observed in the concentration of phosphate, usually with the reverse phase of the oscillations in O_2 (Ono et al., 2001; Watanabe et al., 2003). Similar oscillations in dissolved O_2 have been observed in the Sea of Japan (to the West) (Watanabe et al., 2003), to the South of the Japanese islands into the Pacific (between 250 and 1000m) along the 137°E repeating transect (Takatani et al., 2012). If we interpret these oscillations as having a tidal origin, this implies that long-period variations in tidal mixing play a large and direct role in the marine biogeochemical dynamics of the North West Pacific.

https://doi.org/10.5194/egusphere-2026-5168
Preprint. Discussion started: 11 September 2026

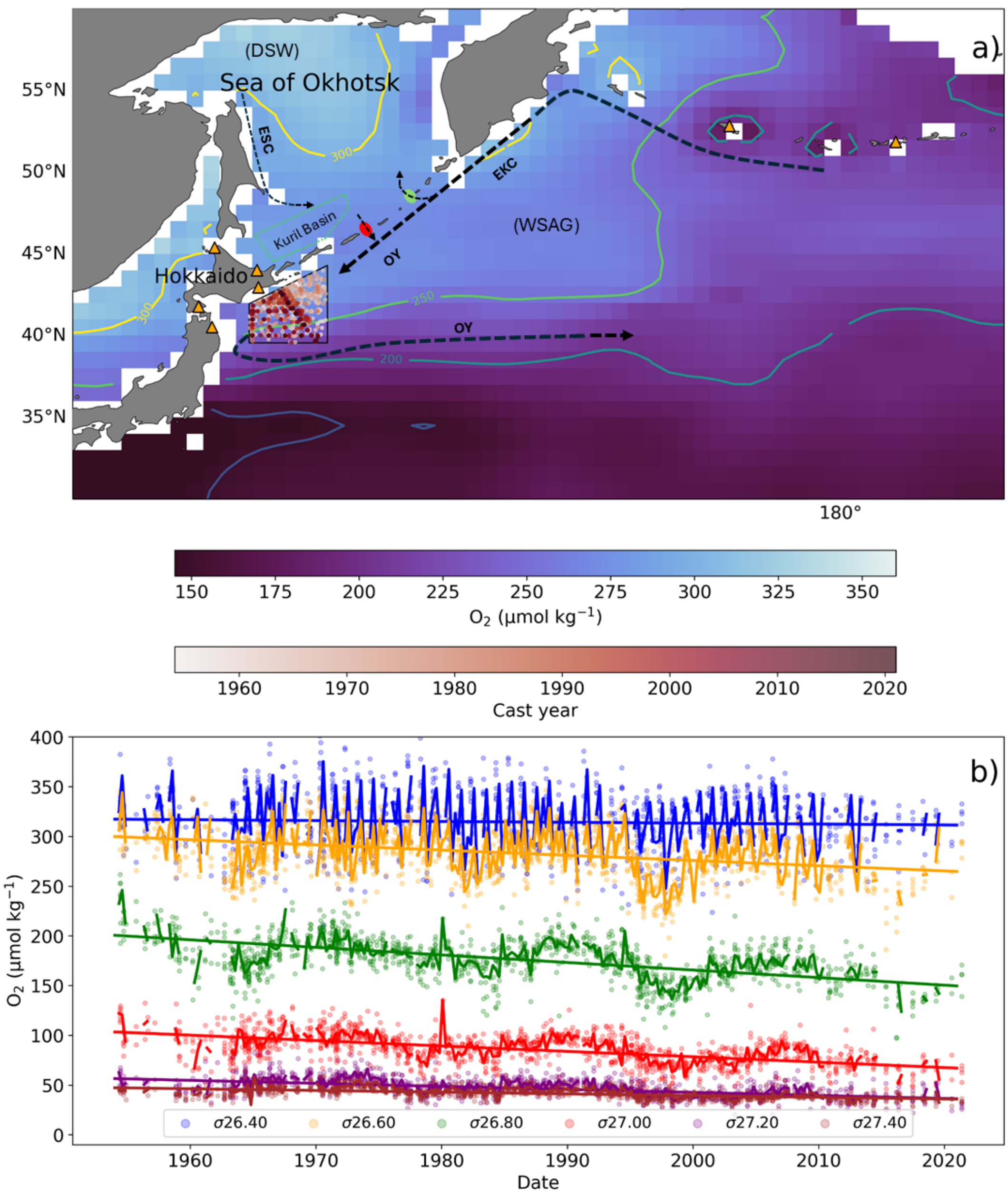

Figure 1. a) The North West Pacific and Oyashio region (black box) and time series observations (points). Background colour and isolines are the climatological O_2 on $26.60\sigma_\theta$ (World Ocean Atlas 2023). Locations of the tide gauges used to derived the tidal index (gold triangles). A schematic representation of the main currents is given by dashed arrows - the Oyashio (OY), East Kamchatka (EKC) and East Sakhalin (ESC) currents. An inflow through the Kruzenstern strait is shown (green point) with an outflow in the Bussol strait (red point). The Western subarctic gyre (WSAG) and dense shelf water forming region (DSW) are marked approximately in brackets; **b)** O_2 times series from the sampling region (points) on selected σ surfaces, with the linear deoxygenation trend (line).

https://doi.org/10.5194/egusphere-2026-5168
Preprint. Discussion started: 11 September 2026

1.2 North Pacific ventilation and the nodal tide

In the North Pacific, the surface-interior potential density difference is too small to permit the deep convection present in the Atlantic (Warren, 1983). This state is due to a small net volume transport (and salt flux) between the subpolar and subtropical gyres and the region's excess of precipitation over evaporation (Warren, 1983; Emile-Geay et al., 2003). To ventilate water masses beneath the mixed layer, therefore, ventilation from subduction through the base of the mixed layer (Portela et al., 2020) and/or remote ventilation must occur. In the North-Western the Sea of Okhotsk (Figure 1a) coastal polynyas drive sea ice (Kitani, 1973; Shcherbina et al., 2004a) and dense shelf water (DSW) formation, ventilating the water column directly (Talley, 1993). The DSW is transported in the East Sakhalin current along the western margin of the Sea of Okhotsk (Fukamachi et al., 2004). It eventually mixes with warmer Western sub-Arctic gyre (WSAG) water and Soya current water, which originates in the Japan Sea (Takizawa, 1982). The WSAG water, meanwhile, entered the Sea of Okhotsk through the Northern Kurils (Figure 1a) undergoing some transformation by tidal mixing (Ohshima et al., 2010). These water masses mix to form Okhotsk sea mode water (OSMW), sometimes referred to as intermediate water. The OSMW remains within the Kuril basin for $\sim$1 year (Ohshima et al., 2010), before flowing to the Pacific through the straits in the Southern Kurils, such as the Bussol strait (Figure 1a). The Oyashio water, the focus of this study (sampled within the region shown in Figure 1a), is a mixture of the outflowing OSMW and WSAG water (Sasano et al., 2018), eventually forming NPIW. Collectively these processes are referred to as the North Pacific "overturning circulation" (Mensah and Ohshima, 2021), transferring the trends and variability in their temperature, salinity and other chemical tracers to the Oyashio region and Pacific interior.

Tidal processes play a fundamental role in the ocean's dynamics, largely by driving diabatic mixing (Simpson et al., 1996; Garrett, 2003), modifying water masses and dissolved tracer distributions with measurable impacts on marine biogeochemistry (Ditkovsky and Resplandy, 2025; Damien et al., 2026), but their effects are most pronounced in the marginal and shelf seas (Simpson et al., 1996; Rippeth, 2005). Tidal mixing within the SO, modulated by the 18.6 year frequency or nodal tide, strongly influences the ocean dynamics at multiple stages of the circulation through the sea (Nakamura et al., 2006; Ono et al., 2006; Gladyshev et al., 2003). The 18.6 frequency arises because the angle of the Lunar declination varies over the precession cycle of 18.6 years (Woodworth, 2012). Because the angle of declination is above and below the equator, the effect of this nodal cycle on the ocean tides is greatest at higher latitudes. Therefore, the barotropic current velocities are maximised in the diurnal frequencies (K1 and O1) when the declination is largest and a minimum once the Lunar declination is zero (in line with the equator). As tidal mixing responds nonlinearly to the barotropic velocity, even small changes in the forcing may have large, measurable consequences for processes which respond to mixing, such as the surface density of sea ice (Ono et al., 2006) and the concentration of O_2.

However establishing an empirical causal relationship from the tide to some process from observations can be challenging. To give an example from climate dynamics: the proposed mechanism for a tide-climate link is a cooling effect on sea surface temperature by tidal vertical mixing. This would alter the air-sea heat fluxes, leaving a tidal 'footprint' in regional and global climate variability (Loder and Garrett, 1978). Keeling and Whorf (1997) suggested that long-period tides might explain millennium-scale climate variability in Earth's past, yet, using dynamical arguments, Munk et al. (2002) then showed the tidal forcing at millennial timescales was unlikely to be strong enough to have such an effect. A tidal explanation was also made for palaeoclimate extremes by Keeling and Whorf (2000) and again later analysis also showed that this to be unlikely (Ray, 2007). The influence of the nodal tide on decadal climate processes is on firmer theoretical ground (Munk et al., 2002; Ray, 2007). Theoretically the nodal tide could induce a small temperature response in the ocean (Garrett, 1979) and numerical modelling by Joshi et al. (2023) showed that a parameterised nodal tide can generate a small global annual surface temperature anomaly. However, Ray (2007) points out that distinguishing pseudo-periodic processes from truly periodic ones, such as a tide in short and noisy time series, is not a trivial task. In oceanic O_2 research this problem is compounded by the sparse spatial and temporal data coverage and the length of oceanographic time series: many of the potential causes of O_2 trends and variability act over time scales over time scales longer than most time series of marine O_2 (Deutsch et al., 2014; Duprey et al., 2024). Additionally, significant correlations between apparently periodic signals and the 18.6 year cycle are often identified in biogeochemical and ecosystem time series in the North Pacific (Yasuda et al., 2006; Whitney et al., 2007; Keeling et al., 2010; Stramma et al., 2020).

Our aim is to establish whether a causal effect from the nodal tide is identifiable in the Oyashio marine biogeochemical time series, explicitly framing the problem in terms of cause and effect rather than association. Furthermore, the use of causal methods on ocean observations remains limited (ie. Navarra et al. (2026)), although there have been recent analyses of numerical ocean model output (Bénard et al., 2025a, b). An investigation of real observations in the context of an observed oceanographic phenomenon (bidecadal oscillations) and its poorly observed causes (tidal mixing, SO dynamics) appears timely. Our general aim can be broken into the following three questions: 1) Can a causal effect from the tide onto O_2 be identified using historical observations? 2) Do the dominant climate modes of the North Pacific provide causal information about the O_2 dynamics in the Oyashio region? 3) If such effects are identifiable, what are their effective lags, density distribution and effect sizes in this system?

2 Method

2.1 Data treatment and preprocessing

We use the dataset compiled by Sasano et al. (2018) to evaluate the O_2 dynamics of the Oyashio region. The hydrographic observations were conducted by the Japan Meteorological Agency in repeat cruises, with the total number of observations per year peaking between the late 1990s and early 2000s (Sasano et al., 2018). This was updated to include the years up to May 2021, but as these years are too sparse for our purposes, we analyse the period between 1954 and 2018. All of the observed quantities from the region (temperature, salinity and oxygen) have been quality controlled, but we will briefly summarise the measurement methods and quality control procedures (see Sasano et al. (2018) and Takatani et al. (2012) for a more detailed discussion). The O_2 concentration was determined using Winkler titration until January 1994 (Takatani et al., 2012; Sasano et al., 2018), at which point modified Winkler titration was adopted (Carpenter, 1965); the analysis precision did demonstrably improve after this point (Takatani et al., 2012). For temperature, mercury reversing thermometers mounted on Nansen bottles were used until January 1989, with Conductivity Temperature Depth instrument packages equipped with a Niskin bottle rosette

https://doi.org/10.5194/egusphere-2026-5168
Preprint. Discussion started: 11 September 2026

not employed until after 1990. Sasano et al. (2018) employ the conservative tracer approach of Broecker (1974) as the primary quality control procedure used to identify outliers due to analytical error (avoiding falsely rejecting natural variability). This was performed for all O_2 time series, as well as temperature and salinity prior to 1989. O_2 observations were rejected if their co-located temperature and salinity samples failed quality control. All observations have been interpolated to potential density surfaces (Akima interpolation (Akima, 1991)), at intervals of 0.05 kg m^{-3}. From here on these surfaces will referred to by σ_θ prefixed by the density value. Evaluating the O_2 concentration in density space should control for much of the local effect of vertical isopycnal displacement, better isolating the remote causes of O_2 concentration variability that are the focus of this analysis. Finally, although the samples are distributed over a relatively large region of ∼1.6e+4 km^2 (Figure 1a), the effect of systematic spatial offsets between cruises is small at ∼3 μmol kg^{-1} (Sasano et al., 2018).

The sensitivity and reliability of many time series causal inference methods can depend on the frequency of missing data within the time series (Camps-Valls et al., 2023). The Oyashio record is relatively sparse (Figure 4a), particular months and even whole years may not be represented. The individual observations themselves are also irregularly spaced in time, a common problem in ocean station records which are typically collected through research cruises. To resolve both issues, we reduce the sparsity of the Oyashio time series by taking seasonal averages (Figure 4b). The averaging does reduce the number of data points and sample size available to the causal discovery method; however, the PCMCI method has been shown to remain robust even in analyses of time series with only a few hundred data points (Runge et al., 2019b). We do not include an O_2 time series from within the SO simply due to a lack of data—the sea is one of the most poorly sampled marginal seas in the world (Mensah and Ohshima, 2021). The period of the nodal tide also approaches the limit of most quasi-continuous ocean time series (∼ 20 years). For the time period covered by this dataset, we only resolve three nodal tidal cycles. Any yearly seasonality was removed with a polynomial fit to all levels above 26.8σ_θ.

The other input variables, illustrated in Figure 3, are climate indices that may be relevant to the O_2 dynamics. Their inclusion in the analysis is based on the existing literature on Oyashio regional dynamics (Sasano et al., 2018; Ito et al., 2019; Stramma et al., 2020). The Pacific Decadal Oscillation (PDO), is defined as the leading principal component of sea surface temperature variability in the North Pacific (Mantua and Hare, 2002). The North Pacific Index (NPI) is an area-weighted sea level pressure index taken over 30°N-65°N and 160°E-140°W (Trenberth and Hurrell, 1994). The North Pacific Gyre Oscillation (NPGO) is the second principal component of sea surface height in the North Eastern Pacific (Di Lorenzo et al., 2008).

The tidal index represents the signal of the nodal cycle present in the diurnal and semi-diurnal tidal frequencies. In reality, however, the nodal tide will affect regional dynamics through tidal mixing around the Kurils, the SO and elsewhere. This is a non-linear process, but the long-period of the nodal cycle allows us to make some strong assumptions about its total causal effect on the O_2 time series "downstream". Because the nodal frequency is so much lower than the diurnal or semi-diurnal frequencies it influences (1/18.6 years versus ∼1/24 hours for the diurnal constituents), the impact of the non-linearities inherent in daily vertical mixing simply scale with the magnitude of nodal cycle at any given phase over its 18.6-year period. This assumption is commonly made when modelling the effect of nodal variation in vertical mixing, by varying a diffusivity by a constant value over the cycle (Osafune and Yasuda, 2013; Joshi et al., 2023). The tidal index is derived from tide gauge records (Caldwell et al., 2015), which are marked in Figure 1b. We only selected gauges with records longer than 9 years. A sea level reconstruction

https://doi.org/10.5194/egusphere-2026-5168
Preprint. Discussion started: 11 September 2026

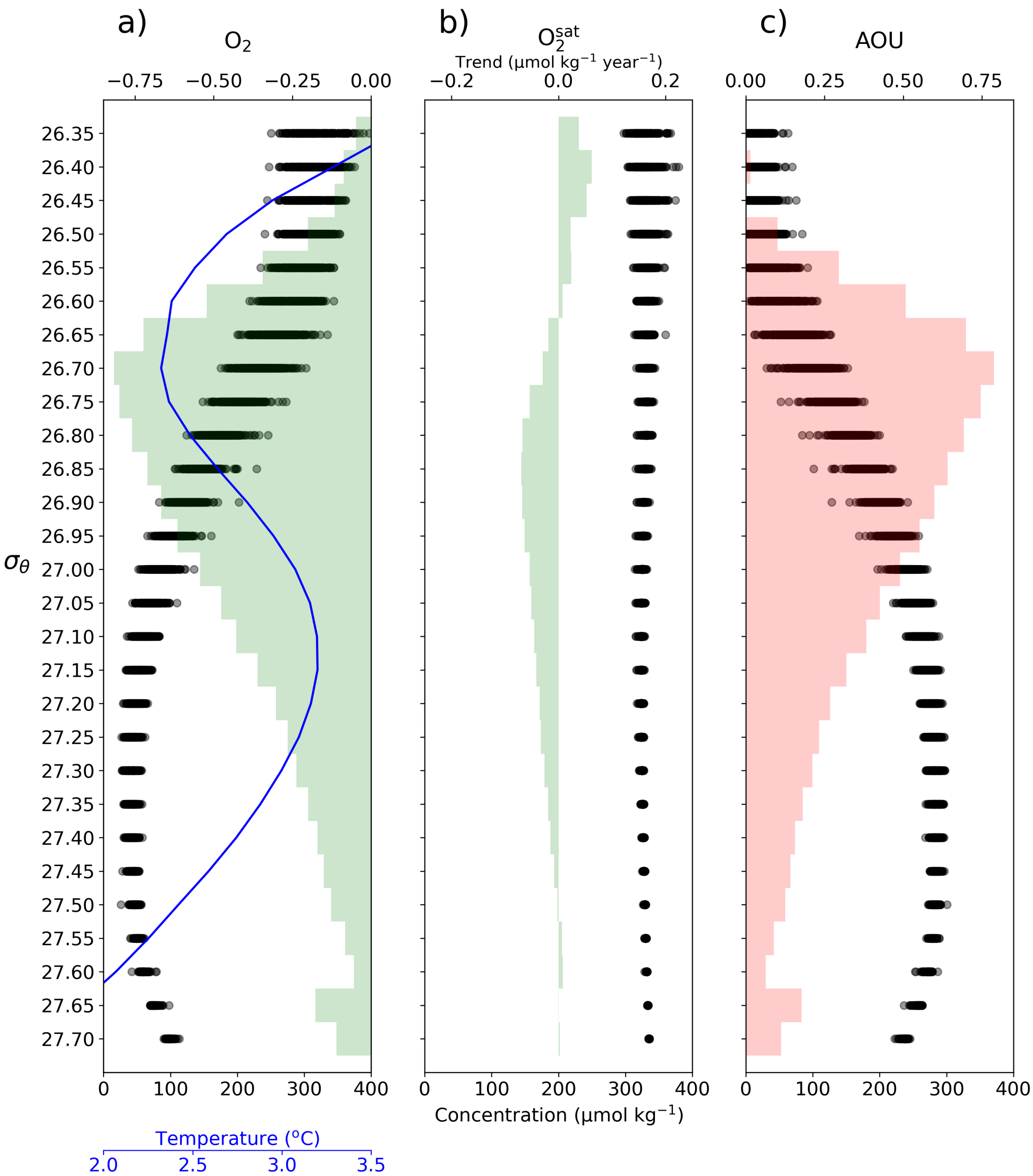

Figure 2. **a)** The distribution of O_2, **b)** O_2 saturation (O_2^{sat}) **c)** apparent oxygen utilisation (AOU) concentration over density (dark points, σ_θ indicates the potential density level), with the linear trends for O_2 and AOU (bars). The trends for O_2 and AOU are found with a linear fit to yearly-mean time series. The temperature climatology over density (blue curve and panel **c**) has a characteristic increase towards the temperature maximum at $\sigma_{27.17}$.

https://doi.org/10.5194/egusphere-2026-5168
Preprint. Discussion started: 11 September 2026

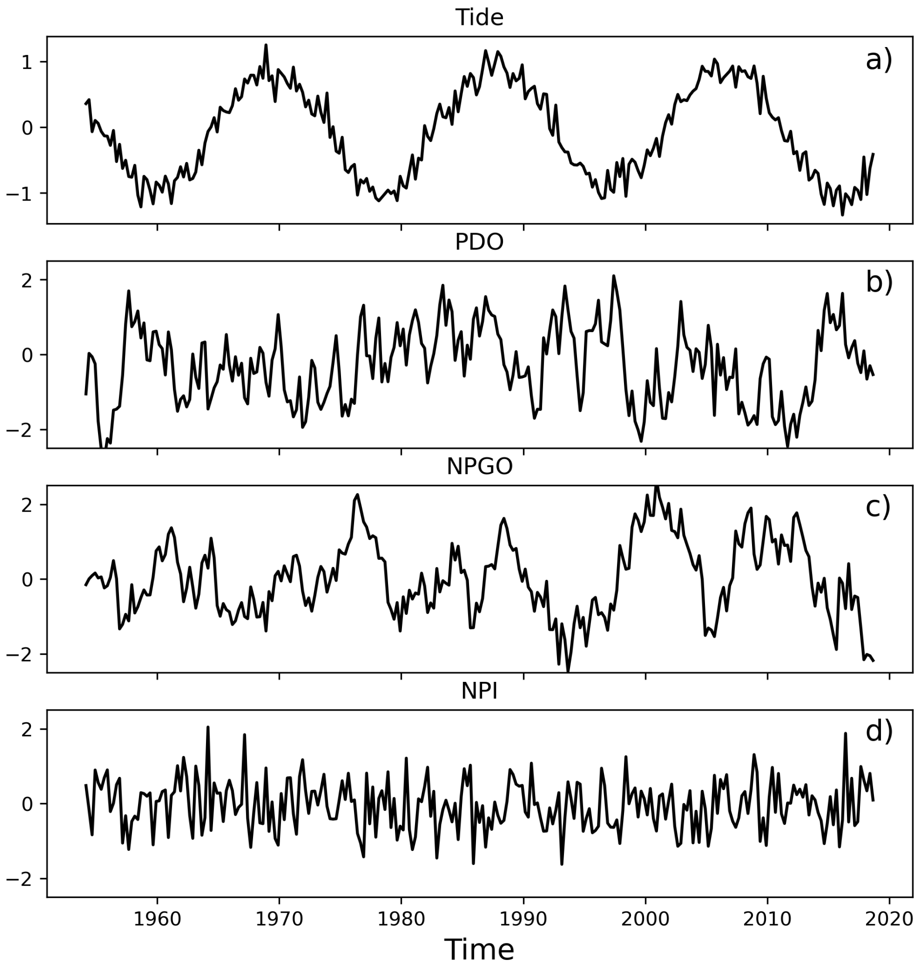

Figure 3. Time series of the potential "drivers" of Oyashio O_2. **a)** The index of the 18.6-year nodal tide. **b)** The Pacific Decadal Oscillation (PDO). **c)** The North Pacific Gyre Oscillation (NPGO). **d)** The standardised North Pacific Index (NPI). Each index is at the same seasonal resolution as the Oyashio time series, or 4 data points per year

https://doi.org/10.5194/egusphere-2026-5168
Preprint. Discussion started: 11 September 2026

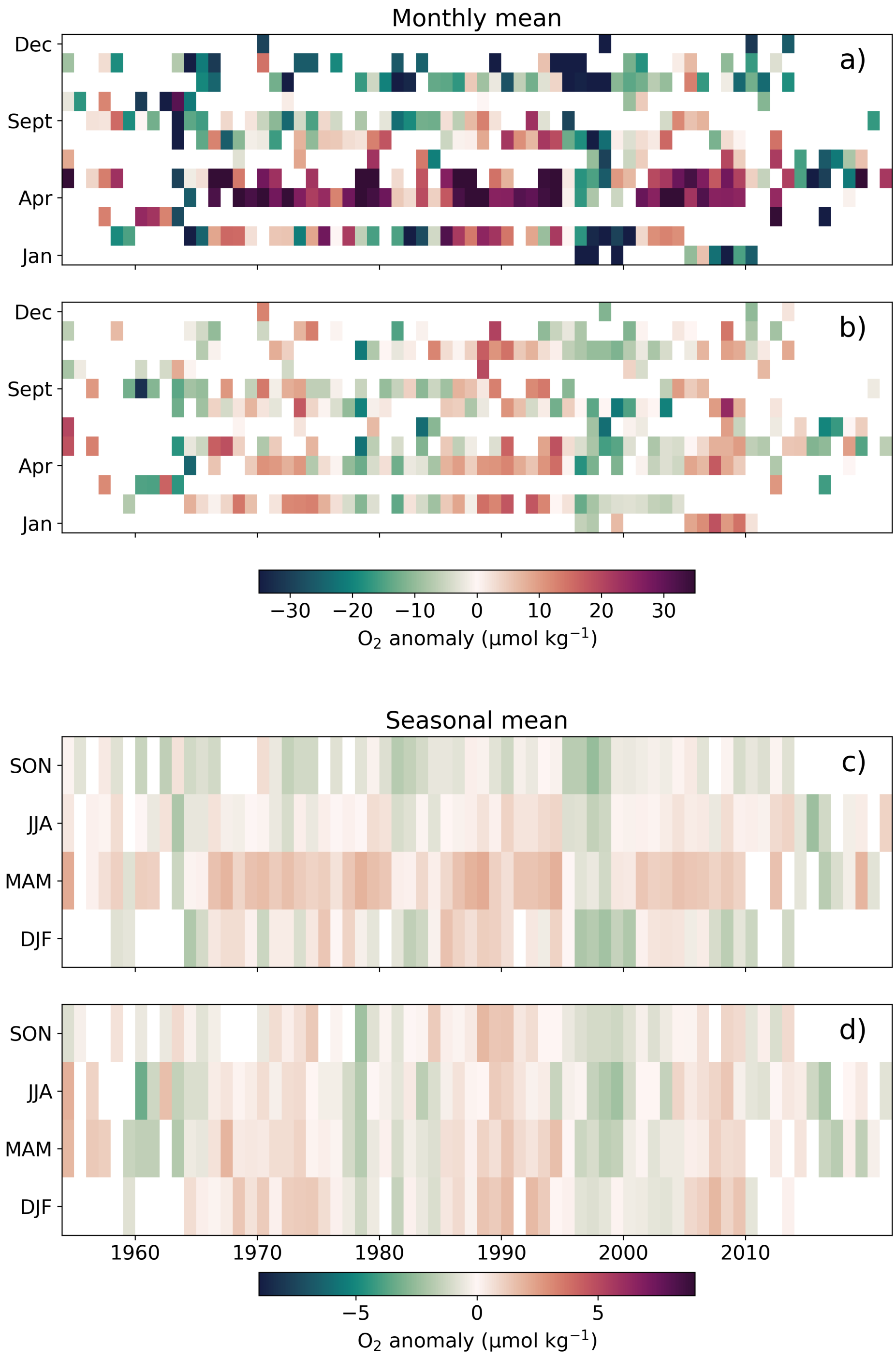

Figure 4. The detrended monthly and seasonal mean O_2 anomalies on two density surfaces $26.60\sigma_\theta$ (**a**, **c**), where the period of net O_2 production in spring is a strong positive anomaly; $27.00\sigma_\theta$ (**b**, **d**), where the apparent 18.6-year tidal signal is clearly visible, and of comparable magnitude to the spring O_2 production.

https://doi.org/10.5194/egusphere-2026-5168
Preprint. Discussion started: 11 September 2026

is found from the dominant constituents for each gauge using UTide (Codiga, 2011). The sea level reconstructions give us the deterministic component of the index (just a cosine of period 18.61 years) and an independent noise term found from the residuals of the sea level reconstruction, terms which are then subsampled and averaged at the required temporal resolution.

2.2 Time series causal discovery

Graph networks already have a history within marine science. In marine ecology, for example, they can be used quantify connectivity between populations (Treml et al., 2008; Abecasis et al., 2023) and assess the impact of human interventions on aquatic ecosystems (Saunders et al., 2015). Graphical causal discovery methods meanwhile, have proven valuable in estimating the causal effects between remote atmospheric processes (teleconnections) (Runge et al., 2015; Kretschmer et al., 2021) and in understanding the causal interactions behind seasonal atmospheric dynamics (Kretschmer et al., 2016). They have been applied to systems where the causes of chemical fluxes may be ambiguous, such as between vegetation and the atmosphere (Krich et al., 2020) or in the concentration of an aerosol pollutant (Kumar et al., 2022). These forms of cause $\rightarrow$ effect problems have been highlighted as an area of growing importance in the study of marine ecosystems (Griffith, 2020). We apply one such time series causal discovery algorithm. This graph has two key components; the nodes, which are the input time series and the vertices which quantify the causal links (in this case) between the nodes. As this is time series causal discovery, a third component is the lag of the causal effect from one node to another. Time series causal discovery methods have been widely adopted in both climate science and meteorology (Runge et al., 2015), but at present there do not appear to be any published examples of these forms of causal inference methods applied in marine science of any kind.

Here we employ the PCMCI algorithm (Runge et al., 2019b). As with all discovery methods, PCMCI requires that a set of general assumptions about the data and the system under investigation be met for a valid causal link to be identified - these are as follows:

1. **Faithfulness**: *Independencies* within the data do not occur by chance, but can be traced back to what is known as a d-separation (Hayduk et al., 2003). Consider the case where X is independent of Y given some other variable Z. X must therefore be d-separated from Y given Z. This is an important graphical criterion which defines causal connection and separation in the graph, allowing us to interpret statistical independence as causal separation.

2. **Causal sufficiency**: The dataset being used to identify the structural causal model (SCM) contains all relevant causal variables. There can be no hidden confounders.

3. **Causal Markov condition**: All probabilistic information that can be found from the system being analysed is contained in its causes.

4. **No instantaneous effects**: There are no causal effects at $\tau = 0$. Some methods do allow for this, but it is a condition of PCMCI.

5. **Stationarity**: As in many time series analysis methods, trends and seasonality must either be removed or explicitly accounted for.

https://doi.org/10.5194/egusphere-2026-5168
Preprint. Discussion started: 11 September 2026

6. **The parametric assumptions** of the conditional independence test applied—these are discussed in the definition of partial correlation (Equation 3). The test chosen depends on the problem at hand.

Causal graphical models are one family of causal inference methods which can discriminate between a direct causal link and an indirect one (Ebert-Uphoff and Deng, 2012). The essential idea is that for some set of random variables (say X,Y and Z), we can test whether they are conditionally independent of each other; Runge et al. (2014) give a concise example of this concept (their Section 5). For time series, the time ordering can then be used to define the causal link and its direction—causation can only be instantaneous or forward in time. To illustrate this with a simple example (we will employ the notation commonly used in the literature): for a multivariate process of interest, $\mathbf{X}$, which has two time ordered component variables (nodes) X^i and X^j - we can test whether X^i at some lag τ, has a causal link to X^j. So $X^i_{t-\tau} \rightarrow X^j_t$ for $\tau > 0$ and if

$$X^i_{t-\tau} \not\perp\!\!\!\perp X^j_t | \mathbf{X}^-_t \setminus \{X^i_{t-\tau}\} \tag{1}$$

where $\not\perp\!\!\!\perp$ indicates a conditional dependence on ("not" independent of) the whole past of the process ($\mathbf{X}^-_t$) only excluding $X_{t-\tau}$. That is, if $X^i_{t-\tau}$ is never conditionally independent of X^j_t, upon conditioning on $\mathbf{X}^-_t$, excluding $X^i_{t-\tau}$ itself, then we conclude that $X^i_{t-\tau}$ is a causal factor for X^j_t. As long as $X^i \neq X^j$, the link $X^i_{t-\tau} \rightarrow X^j_t$ is a causal link from $X^i_{t-\tau}$ to X^j_t. Otherwise this would be an auto-dependency—a causal link to itself, at lag τ.

A detailed proof of the PCMCI algorithm and pseudo-code can be found in (Runge et al., 2019b), but we will give a qualitative summary of the key components. From causal discovery theory (Pearl, 2009a; Spirtes et al., 2001), the causal parents, $\mathbf{P}(X_t)$, of a given variable, X_t, can be considered as a sufficient conditioning set which allows us to establish conditional independence between X_t and any other variable that is not a causal descendent of X_t. In other words, all causal information for a variable can be found within its parents, as implied by the causal Markov condition (Condition 3, Section 2.2). PCMCI operates in two parts: First, the PC algorithm is applied as a skeleton discovery step (Colombo et al., 2014) to identify a set of potentially relevant conditions, $\widehat{\mathbf{P}}(X_t)$, a subset of $\mathbf{X}$ that should contain both the true causal parents and a number of false positive links. The PC step thereby reduces the dimensionality of the problem, reducing the size of space that needs to searched to identify the causal parents. The second part is where the conditional independence test is applied and the algorithm determines whether $X_{t-\tau} \rightarrow Y_t$. Specifically, this is known as the MCI test which establishes the link $X^i_{t-\tau} \rightarrow X^j_t$ if

$$\textbf{MCI} \; : X^i_{t-\tau} \not\perp\!\!\!\perp X^j_t \mid \widehat{\mathbf{P}}(X^j_t) \setminus \{X^i_{t-\tau}\}, \widehat{\mathbf{P}}(X^i_{t-\tau}) \tag{2}$$

where we can see that the MCI test also conditions on the time-lagged parents of X^i_t, $\widehat{\mathbf{P}}(X^i_{t-\tau})$, accounting for any auto-dependencies and improving the algorithm's ability to control for false positives. The conditional independence test applied here is linear partial correlation, as we make the assumption of linear causal links and independent gaussian noise for all variables analysed at each density level. The PCMCI method can, however, also be applied with non-linear conditional independence tests (Runge et al., 2019b). For reference, partial correlation assumes the model:

https://doi.org/10.5194/egusphere-2026-5168
Preprint. Discussion started: 11 September 2026

$$X^i = \beta_i \widehat{\mathbf{P}}(X^i) + \eta^i, \quad X^j = \beta_j \widehat{\mathbf{P}}(X) + \eta^j \tag{3a}$$

$$R^i = X^i - \widehat{\beta}_i \widehat{\mathbf{P}}(X^i), \quad R^j = X^j - \widehat{\beta}_j \widehat{\mathbf{P}}(X^j) \tag{3b}$$

with R being the residuals between the variable and the conditioning set, $\widehat{\mathbf{P}}(X)$ from the PC step, η is an independent noise term. The effect of $\widehat{\mathbf{P}}(X)$ on X^i and X^j is removed with ordinary least squares regression, whose coefficient is given by the estimated β, denoted by $\widehat{\beta}$. The residuals R^i and R^j are then tested for independence with Pearson's correlation and a t-test; i.e. is the correlation then significantly different from zero? In a sense, this is an linear regression analysis, but one that makes stricter assumptions about when an apparent link between variables should be considered causal.

2.3 Application of PCMCI to the Oyashio dataset

We apply the PCMCI causal discovery algorithm to the dataset from (Sasano et al., 2018). The time series of O_2, AOU and O_2^{sat} are evaluated as anomalies and are standardised by month. This allows for a comparison of the causal links between σ_θ levels that controls for their respective mean dissolved O_2 concentration, i.e. 26.70σ_θ has a mean O_2 concentration ∼200 μmol kg^{-1} greater than 27.00σ_θ. We also make a unique assumption in addition to the methodological requirements of PCMCI: that there is no causal link between the density levels at this seasonal resolution, so all levels can be evaluated as independent graph networks. This is for two reasons: First, because the quantities of interest here have been interpolated onto σ_θ levels, the values on a given level will be an instantaneous function (a function at t=0) of the surrounding levels, adding artificial causal effect. Second, arguing from dynamics, any physical relationship between a scalar quantity on two isopycnals can only be caused by some form of mixing, we will assume that local mixing effects are negligible. Additionally, even though O_2 and O_2^{sat} are derived from independent measurements, because any one of the input variables is defined as a linear combination of the other two ($O_2 = O_2^{sat} - \mathrm{AOU}$), we cannot analyse them in the same graph, as PCMCI cannot distinguish between deterministic copies of variables.

For all density levels, we run the analysis with $\tau_{min} = 1$, $\tau_{max} = 12$, and $\alpha = 0.01$. Although the choice of these parameters will always depend on the form of the data and system being analysed, we do test different values of τ_{max} and repeat analysis with a less stringent $\alpha = 0.05$. Additionally, to control the false-discovery rate (of false positive causal links), each implementation of PCMCI is run with a Benjamini-Hochberg test for multiple comparisons (Benjamini and Hochberg, 1995).

3 Results

3.1 The nodal tide causally influences dissolved oxygen and AOU

Deriving a graph with causal discovery makes the interpretation of which variables cause some effect on another considerably more straightforward. Figure 5a, c and d are a set of graphs illustrating the causal links from the tidal index for one density level for each of our target variables (27.00σ_θ). The causal link from the tidal index at a single lag (8 season units or ∼2

https://doi.org/10.5194/egusphere-2026-5168
Preprint. Discussion started: 11 September 2026

Table 1. Interpretation of quantities used to characterise the causal influence of one variable on to another - here the example is the tidal influence on O_2.

In-text quantity	Notation	Interpretation
Causal link	$\mathrm{NT}_{t-\tau} \rightarrow \mathrm{O}_{2,t}$	A directed relationship identified by PCMCI using the MCI conditional-independence test - binary, as a link was or was not identified
Link strength	$\mathrm{MCI}(\mathrm{NT}_{t-\tau}, \mathrm{O}_{2,t} \mid \widehat{\mathbf{P}}(\mathrm{O}_{2,t}))$	The strength of the conditional dependence remaining after accounting for the relevant causal parents. In this analysis, this is estimated using linear partial correlation. Takes on a value between 1 and 0.
Causal effect	$\beta_{\mathrm{Tide} \rightarrow O_2}$	The effect of an intervention on the tidal index on O_2, estimated from the corresponding structural causal model. With standardised variables, the coefficient gives the change in O_2 standard deviations resulting from a one-standard-deviation intervention on the tidal index.

years) is clearly identified for both O_2 and AOU. No significant causal link could be identified from the tidal index on to O_2^{sat}. We also include graphs of the links found with a lagged correlation (panels b, d and f), to provide a comparison to a form of associational analysis that is often employed in observational oceanography. The graphs identified by PCMCI are far sparser than those found with lagged correlation, and while this system is not especially complex (it is not a "high dimensional" system consisting of a large number of variables and lags), the graphical results are easier to interpret, limiting post-hoc justification of causal links. These correlations can be physically meaningless if interpreted causally, such as the links from $O_2$to the tidal index. It also is less clear which lags might be chosen for model fitting - all? or a subset selected by the researcher? In less stringent analyses, such as those lacking a false discovery rate control for example, considerably more links can be "discovered" (Figure A1b,d,f). Indeed, without the FDR used here, we can also identify significant statistical links from the climate modes on to our target time series (see Figures A2b to A4b), relationships which have been previously identified in the literature (Watanabe et al., 2003; Ito et al., 2019; Stramma et al., 2020). These effects do seem to be sensitive to the choice of α (Section 3.5).

3.2 The tidal effect has a clear density and lag structure

By evaluating each density surface as a separate causal network, we can investigate how the causal links vary over density — given our assumption of independence between the σ_θ levels. Figures 6 to 8 illustrate the distribution of the maximum causal

https://doi.org/10.5194/egusphere-2026-5168
Preprint. Discussion started: 11 September 2026

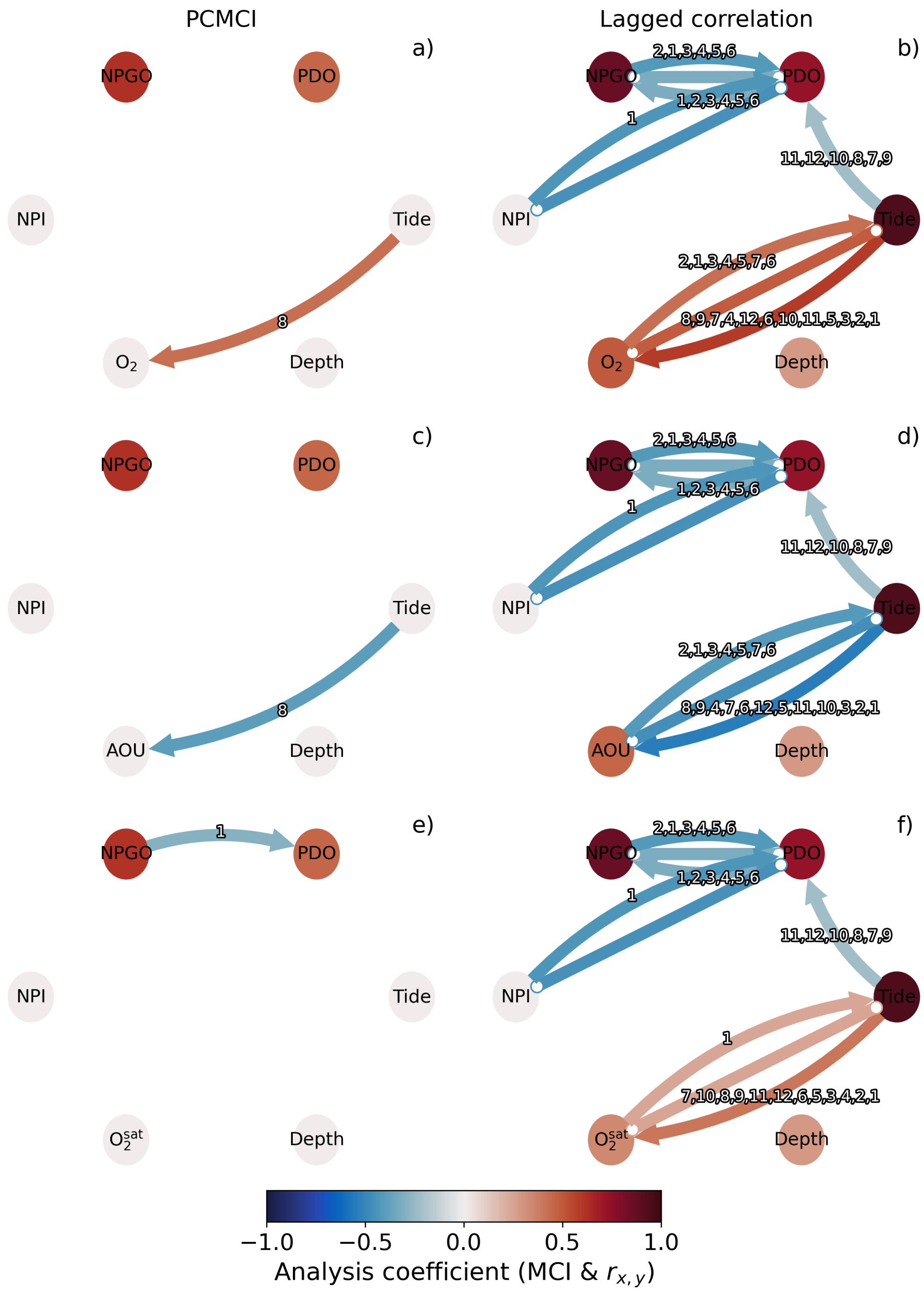

Figure 5. An example of causal (**a, c, e**) versus correlational (**b, d, f**) graphs for dissolved oxygen (**a, b**, O_2), apparent oxygen utilisation (**c, d**, AOU) and the solubility of oxygen (**e, f**, O_2^{sat}) from $27.00\sigma_\theta$. Node and arrow colours indicate the maximum of the mutual conditional information value (MCI) or lagged-correlation coefficient. The numbers on the arrows are lags in units of seasons, ordered according to the value of the coefficient (causal or correlational) - largest first.

https://doi.org/10.5194/egusphere-2026-5168
Preprint. Discussion started: 11 September 2026

Table 2. Summary of the density distribution of the correlational and causal links from the tidal index to the target variables, $\alpha = 0.01$

Analysis	**Variable**	**ID'd σ_θ range (kg m^{-3})**	**Max' coeff' [95% CI of max coeff'], σ_θ level**	**Max' lag (τ)**
	O_2	1.3 (26.4 to 27.70)	0.66 [0.60, 0.71], 26.75	8
Lagged correlation	AOU	1.1 (26.5 to 27.60)	-0.65 [-0.71, -0.58], 26.75	8
	O_2^{sat}	0.6 (26.85 to 27.45)	0.40 [0.28, 0.50], 27.00	12
	O_2	0.6 (26.75 to 27.35)	0.46 [0.35, 0.55], 27.10	8
PCMCI	AOU	0.6 (26.75 to 27.25)	-0.43 [-0.53, -0.31], 26.80	8
	O_2^{sat}	—	—	—

link strength (the maximum MCI value) for each density level (panel **a**) alongside the naive lagged correlation (panel b), for comparison. We summarise the key patterns in density in Table 2. The close relationship between O_2 and AOU remains if $\alpha = 0.01$, as the distribution of causal links for AOU is approximately the inverse of O_2. They are not exact opposites however, with a slightly stronger causal link from the tide on to O_2 than AOU (MCI ≈0.4 versus ≈0.3). Under a relaxed $\alpha = 0.05$ (Figures A2a and A3a) we can see a clear asymmetry, which is not apparent in the lagged correlations (Figures A2b and A3b). The use of PCMCI on O_2^{sat} leaves us with very few detections at all, in contrast to the lagged correlation.

For both O_2 (Figure 6a) and AOU (Figure 7b) the density range of significant causal link detections is greatly reduced - specifically, no causal links are identified above $26.75\sigma_\theta$ despite the presence of significant correlations at and above these levels. The dashed line at $26.80\sigma_\theta$ is included as an approximate reference to the density class of the base of the late winter mixed layer, indicating that tidal effects within the mixed layer densities largely vanish. For O_2 and AOU, this reduces the number of detections per density level by about half compared to the lagged correlation examples (Table 2). Figures 6 to 7 show the maximum coefficients, so it is clear that PCMCI reduces the maximum identified effect of the tidal index on to the O_2 and AOU. The density level of the maximum causal link also changes for O_2, but interestingly not for AOU. The link strength is again reduced, with a larger uncertainty at greater a density ($27.10\sigma_\theta$), again well below the mixed layer, compared to the lagged correlation (Figure 6).

In addition to simplifying the relationships between variables, the causal links here are also sparse in time. While we do not show this for all density levels, most levels undergo a simplification of the lag structure as in Figure 5. For both O_2 and AOU the lags of the effect on O_2 have converged to ∼2 years (8 season units), the same as the typical lag in the correlational analysis (Figure 6b and Figure 7), which is also consistent with the original lag values from Sasano et al. (2018).

Several of these results arise from known properties of PCMCI. 1) Figure 5 shows that the autocorrelation present in the lagged correlation is removed by PCMCI, 2) the MCI values are reduced relative to the naive correlation, 3) the density distribution of the causal effects then shifts to greater densities. These results all occur as PCMCI controls for the past of

https://doi.org/10.5194/egusphere-2026-5168
Preprint. Discussion started: 11 September 2026

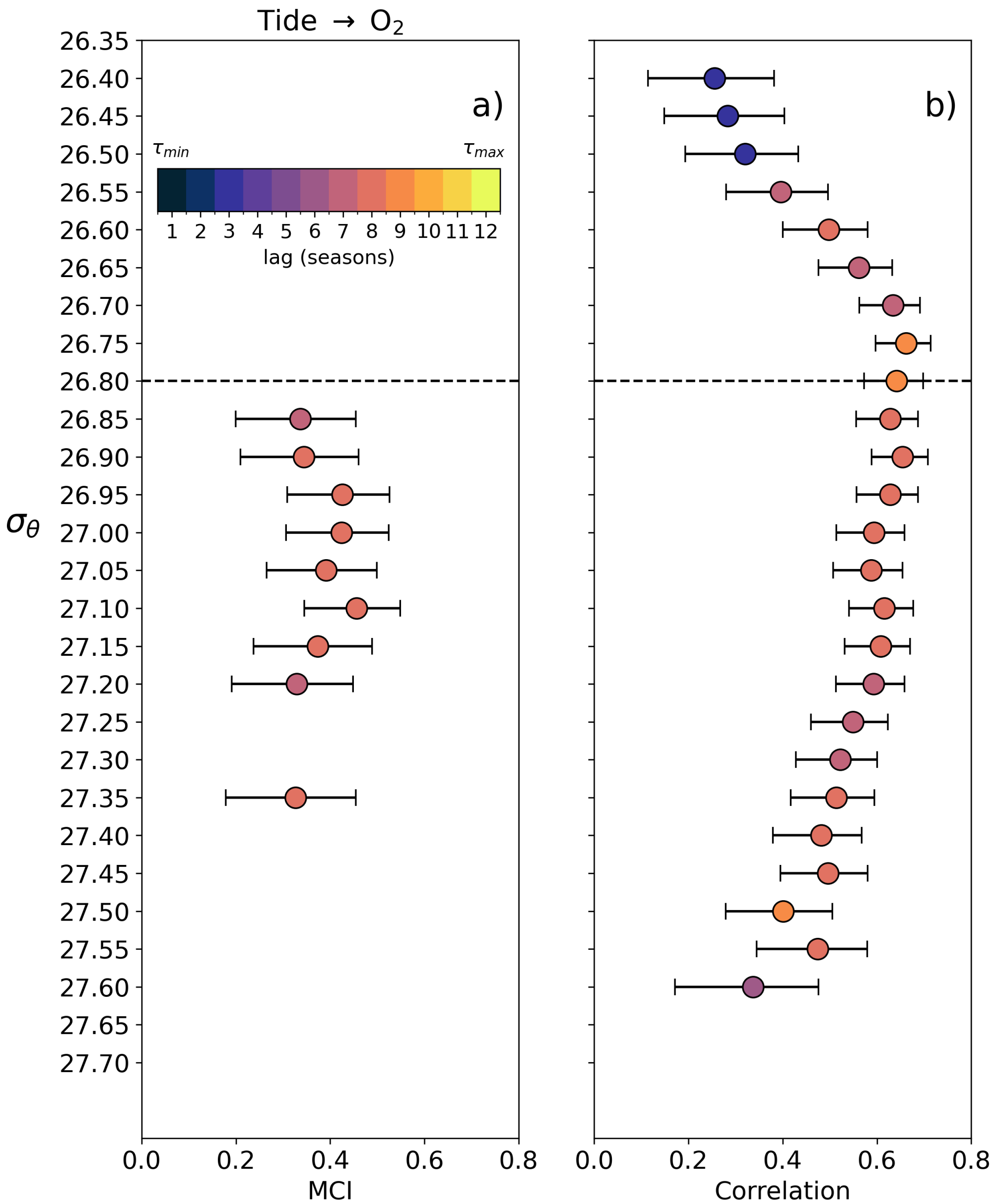

Figure 6. The distribution over density (σ_θ) of **a)** causal links over time from the nodal tidal index to the dissolved oxygen (O_2) time series ($\alpha = 0.01$), **b)** the lagged correlation coefficient. In both a) and b) error bars indicate the 95% confidence interval. The lag magnitude (τ), is given by the colour scale in units of seasons. The dashed line indicates the approximate maximum density reached by the late-winter mixed layer.

https://doi.org/10.5194/egusphere-2026-5168
Preprint. Discussion started: 11 September 2026

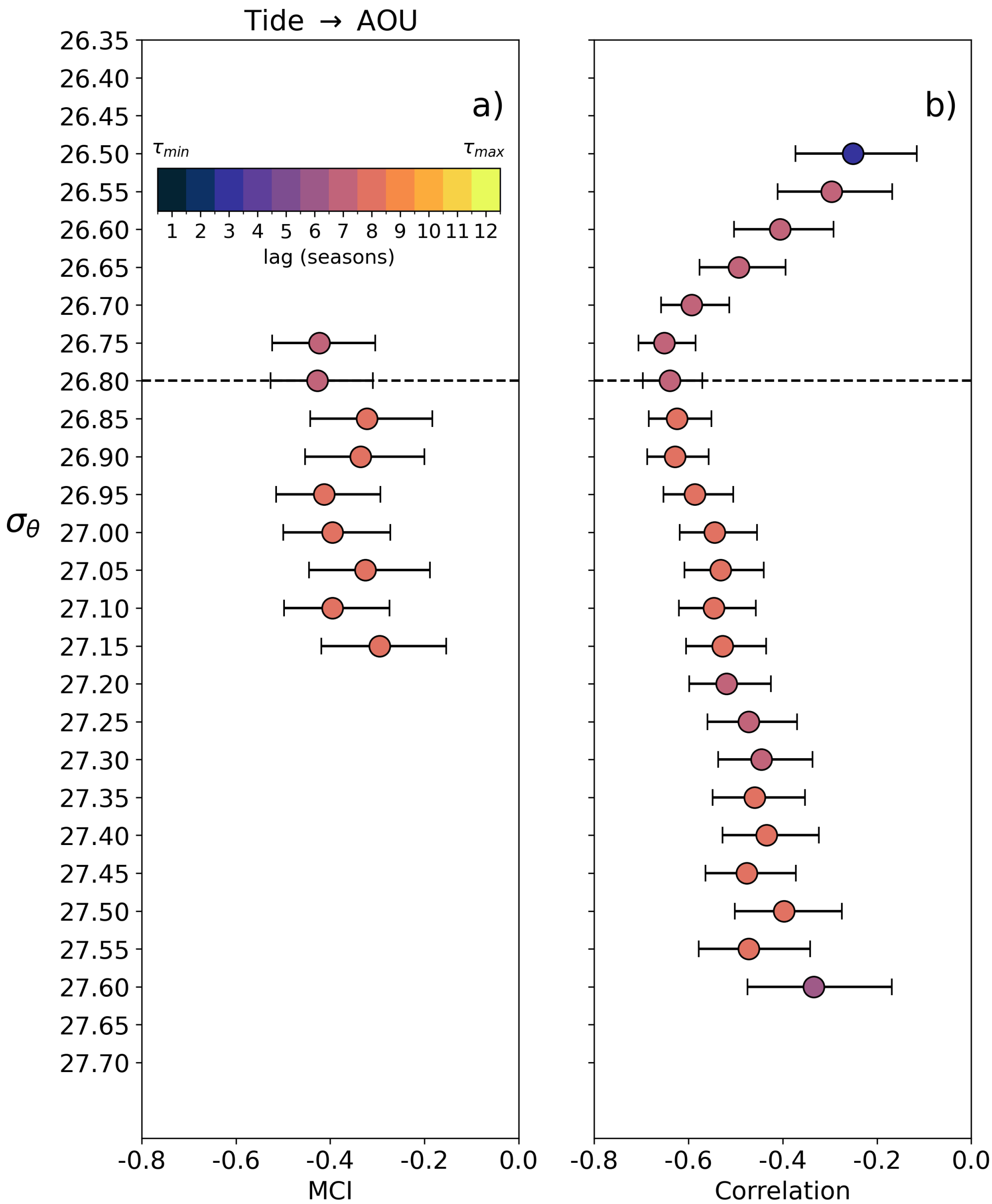

Figure 7. The distribution over density (σ_θ) of **a)** causal links over time from the nodal tidal index to the apparent oxygen utilisation (AOU) time series ($\alpha = 0.01$), **b)** the lagged correlation coefficient. In both a) and b) error bars indicate the 95% confidence interval. The lag magnitude (τ), is given by the colour scale in units of seasons. The dashed line indicates the approximate maximum density reached by the late-winter mixed layer.

https://doi.org/10.5194/egusphere-2026-5168
Preprint. Discussion started: 11 September 2026

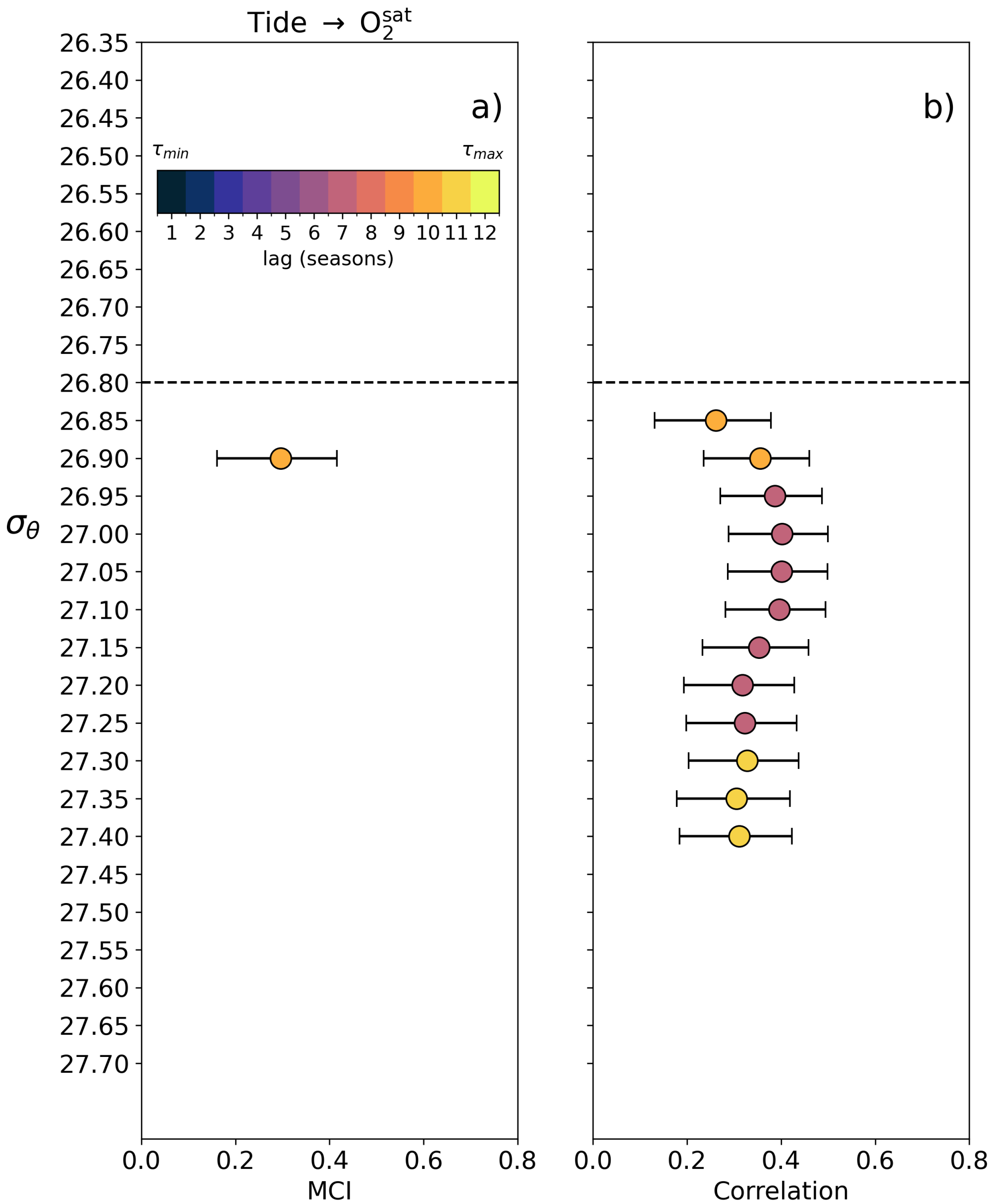

Figure 8. The distribution over density (σ_θ) of **a)** causal links over time from the nodal tidal index to the oxygen solubility (O_2^{sat}) time series ($\alpha = 0.01$), **b)** the lagged correlation coefficient. In both a) and b) error bars indicate the 95% confidence interval. The lag magnitude (τ), is given by the colour scale in units of seasons. The dashed line indicates the approximate maximum density reached by the late-winter mixed layer.

https://doi.org/10.5194/egusphere-2026-5168
Preprint. Discussion started: 11 September 2026

the time series, conditional on the other potential causal parent variables (Runge, 2020) - the test is whether the past of, for example, the O_2 time series contains any information not accounted for by the other causal parents. There are two plausible cases where this can happen. The tidal index (the driver of O_2 and AOU) is a strong, temporally persistent process the almost entirely explains the variation in O_2 or AOU in the Oyashio region, ie: $\mathrm{NT_{t-2}} \rightarrow \mathrm{NT_{t-1}} \rightarrow \mathrm{O_2, t}$. Alternatively the auto-dependency, a causal effect from the past of a variable on to itself, in O_2, AOU and O_2^{sat} does exist (produced by transport or mixing processes for example), but because the effect of the tidal index is large, the residual association is small, so it is discarded. In summary, O_2 time series can be strongly autocorrelated, but the only thing this value implies is predictability, it does not provide causal information per se. PCMCI may remove this effect if a cause or set of causes is "strong", such as our tidal index. This methodological attribute changes the distribution of tidal effects over density considerably, but it is arguably a better estimate of the tide on to O_2, AOU (or not, for O_2^{sat}) in that density class, if the relationship of interest is the tidal causal effect.

3.3 The lagged correlations are explained by the causal model

We can use the causal parents derived from the discovery stage to fit a linear SCM (Runge et al., 2015). It is worth highlighting that this is a sparse model, rather than a more typical auto-regressive model, as we only fit to the identified causal parents rather than the whole past of the process. This will possess the same noise distribution and, most importantly, causal structure of the real dataset. If our assumptions hold (Section 2.2), then we can recreate the correlational relationships of the dataset. Focusing again on a single density level, 27.00σ_θ, we can define the following SCM for O_2 using the maximum effect found at that density level (Figure 6a)

$$\mathrm{O_2^t} := \beta_{\mathrm{Tide}\rightarrow \mathrm{O_2}} \mathrm{NT^{t-8}} + \eta^{\mathrm{t}} \quad (4)$$

Our values of β are found from the linear model fitted to the causal parents of the assignment variable, which is just the tidal index NT here, and η^τ is a noise term that subsumes the variance not accounted for by the causal parents - in this case it is a gaussian with zero mean the same noise variance as the original time series. As these are found from standardised time series, the coefficients can be interpreted as a change of one s.d. unit in a response variable, due to a change in one unit of the parent variable (Kretschmer et al., 2021).

The ensemble of reconstructed lagged correlations for 27.00σ_θ, shown for the two key causal links for O_2 (Figure 9), are in good agreement with the original lagged correlations for this density level. These are the same correlation values illustrated in Figure 6b. This agreement supports the assumptions outlined in Section 2.2 - the causal parents identified by PCMCI, the tidal link and an auto-dependency, can adequately explain the correlational structure when acting within a time series of a comparable standard deviation. The other variables included for each density surface do have causal parents, but these are entirely in the form of an auto-dependency (the node colour illustrated in Figure 5a to c). These auto-dependencies clearly matter in both the climate indices and the isopycnal depth, the other key Oyashio region variable. Generating the same form of ensemble for these variables indicates that, in most cases, an SCM consisting solely of the causal parents and a noise term is

https://doi.org/10.5194/egusphere-2026-5168
Preprint. Discussion started: 11 September 2026

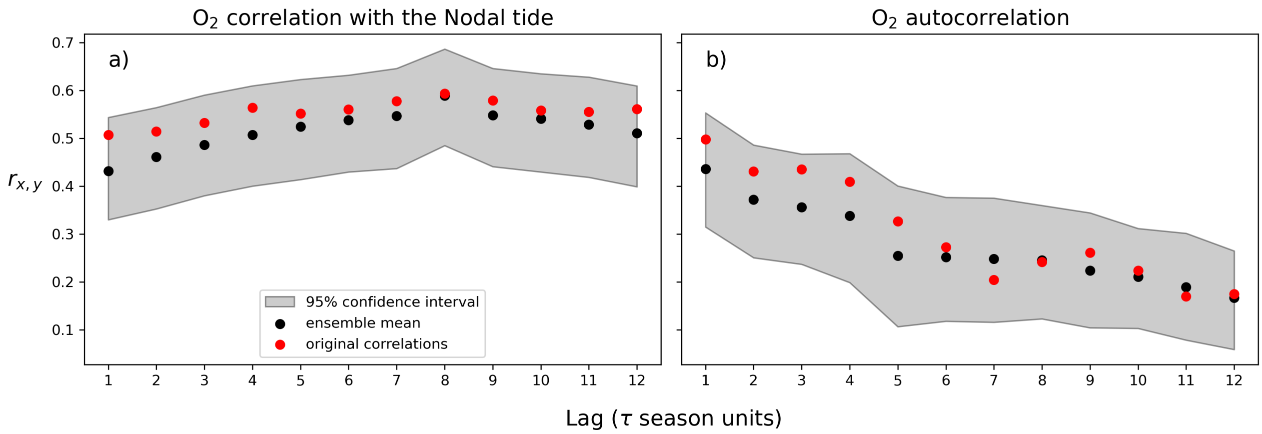

Figure 9. The original and reconstructed lagged correlations on 27.00σ_θ between the nodal tidal index and **a)** the dissolved oxygen (O_2) time series on 27.00σ_θ **b)** The autocorrelation of the O_2 time series. 500 ensemble members were used to generate the confidence intervals

sufficient to explain the correlations between these variables (Figure 10). Indeed in most cases, the original correlations present are indistinguishable from those we would expect between unrelated variables of the same standard deviation.

3.4 Climate modes do not provide additional causal information at seasonal resolution

Previous work on the O_2 dynamics of the Oyashio region makes predictive use of the climate indices we applied in this analysis (Watanabe et al., 2003; Ito et al., 2019; Stramma et al., 2020). We gave some discussion of why the indices may encode information relevant to the O_2 dynamics in the Oyashio region in Section 2.1. Although there are no causal links between these indices, we do find significant seasonal correlations between the indices (Figure 5b,d,f) and mechanistic explanations for their relationships do exist (Di Lorenzo et al., 2008). To briefly summarise their relationships: the NPI is an index of sea level pressure over the North Pacific, so may be related to the NPGO (sea surface height) through the wind stress. The PDO, as a sea surface temperature index, should also respond to the NPI through its dependence on seasonal and subseasonal weather over the North Pacific. Additionally, previous work suggested a nodal tidal link to each these climate indices (Yasuda et al., 2006). We do recover correlations between the tidal index and the PDO (see Figures A2 and A3), but not causal links. So, we are left with two questions to answer: First, why does PCMCI not identify causal relationships between the climate indices if seasonal correlations exist? Second, does a causal link from the nodal tide to any of the climate indices exist?

Seasonal mean data is too coarse to distinguish relationships which take place over 1 to 2 months (see the assumptions required by PCMCI). The causal analysis of aggregated data (ie. time series of mean values) is an area of active research (Wahl et al., 2023), so analysing aggregated time series with current methods may require the user to allow instantaneous (links at $\tau = 0$) and/or unoriented causal links, links which can be identified, but their direction is not identifiable. We use a modified version of PCMCI, PCMCI+ (Runge, 2020), a form that permits instantaneous causal links (we can ignore Condition 4 that is required by PCMCI, see Section 2.2 for method and parameter assumptions), to the original monthly form of the climate

https://doi.org/10.5194/egusphere-2026-5168
Preprint. Discussion started: 11 September 2026

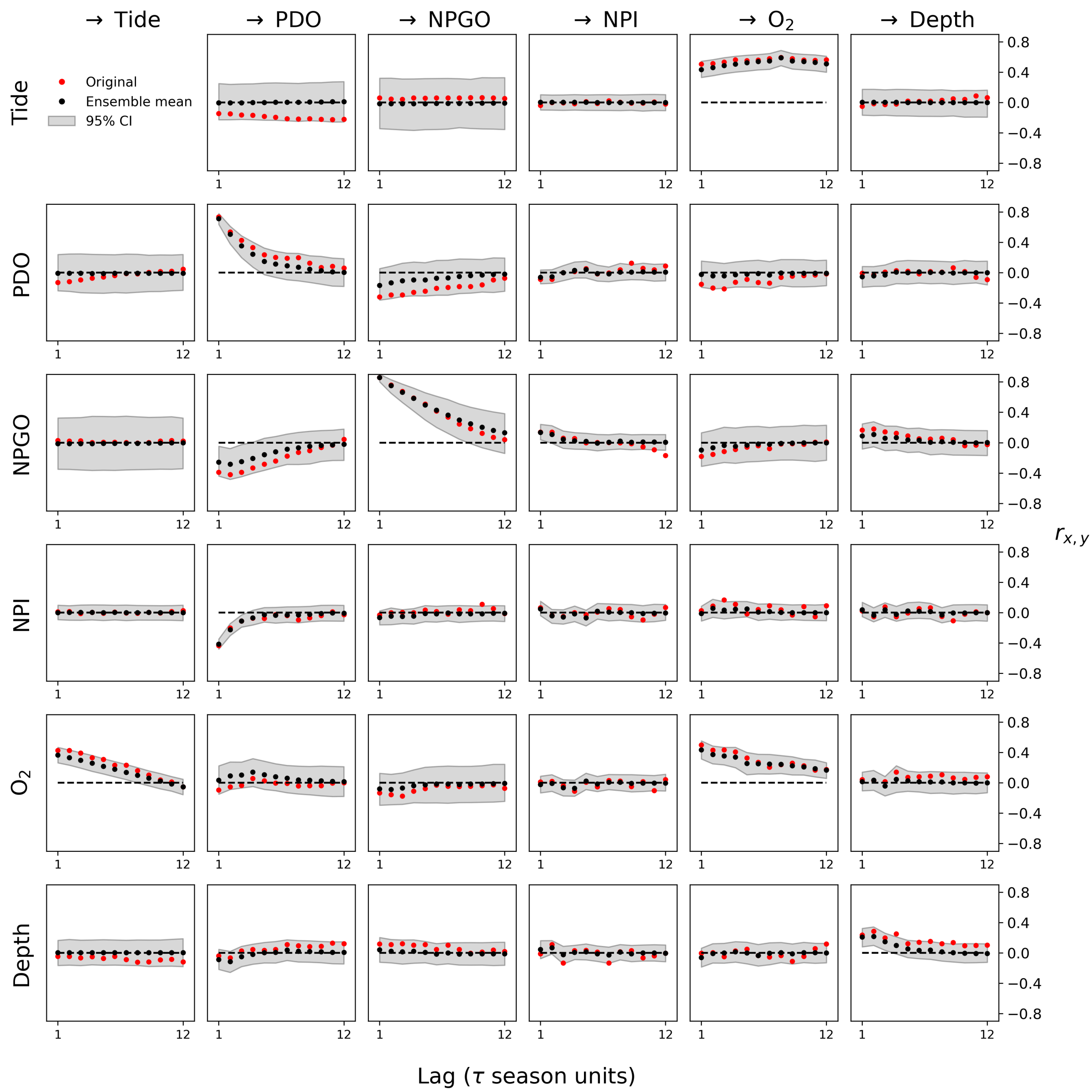

Figure 10. The original (red) and mean of the ensemble of reconstructed lagged correlations (black) between all of the input variables on $27.00\sigma_\theta$. Tide being the tidal index, then the Pacific decadal oscillation (PDO), North Pacific gyre oscillation (NPGO), North Pacific index (NPI), dissolved Oxygen (O_2) and the isopycnal depth (depth). Grey shading indicates the 95% confidence interval

indices and a monthly tidal index (Figure 11a). The tidal index is separable into a purely periodic component and a noise component, allowing us to explicitly test the effect of removing the tide (Figure 11b). To consider the effect of sampling on the discovery of causal links, we employ a bootstrap aggregation approach (Figure 11c) to define a confidence measure of the links using majority voting (see Debeire et al. (2024)). The arrow thickness in Figure 11c is proportional to the frequency of link occurrence. The main causal links between the indices are from the NPI, with an instantaneous link to the NPGO and PDO as well as a weaker lagged link at $\tau = 1$ month on to the PDO (Figure 11a,b), these results are insensitive to different values of τ_{max}. However we do identify a significant, albeit weak, effect from the tide on to the PDO at a lag of $\sim$1.75 years. With the NPI as the sole causal parent (other than auto-dependencies), the negative correlations with the other indices now make sense - a negative effect from the NPI exists, but at a short time scale (Figure 10). The effect from the tide on to the PDO is likely a product of sampling (Figure 11c).

3.5 Sensitivity to parameter choice and the method's assumptions

There are a small number of free parameters governing PCMCI; the τ_{min} and τ_{max}, the value of α and potentially a set of assumptions about the possible causal relationships supplied by the researcher. As many real time series will contain some form of auto-dependency starting in the recent past, $\tau = \tau_{min} = 1$, there is little sense in testing this value. For τ_{max}, different values could be chosen. But as long as the lags of the true causal effects are less than the chosen τ_{max} and sufficient samples are available, the causal links should be identifiable (Runge et al., 2019b). In this analysis, shortening the τ_{max} to 9 season units had little effect on the values of the links shown in Figures 6a and 7a, but lengthening τ_{max} results in there being too few samples available from the time series to achieve a valid result. It is possible to prescribe whether or not particular causal links should exist, and at what lag - but we make minimally restrictive assumptions, any link can exist between nodes, with the exception of the tidal index which can only be a causal parent (Section 2.2).

This leaves us with the sensitivity of the α value. Because α is the significance threshold at which a causal link will be selected, increasing it will allow PCMCI to identify more links. However, because PCMCI is optimised to avoid conditioning on irrelevant variables (see Section 2.2), links selected at $\alpha = 0.01$ should just be a subset of those selected at a less stringent value, for example $\alpha = 0.05$. In this case, we do find some additional density levels with tidal links for both O_2 (Figure A2a) and AOU (Figure A3a), but the general distribution does not change. We do not, for example, find new maximum MCI values at different lags within the density that we have identified as tidally-influenced. For O_2^{sat} , relaxing α returns a set of links absent at α = 0.01. These new links might suggest that selection at the 1% level was too conservative for this dataset.

4 Discussion

Causal graphical networks are a powerful and easily interpreted family of methods for the analysis of high-dimensional systems (Runge et al., 2015, 2019b, a), which are common in oceanography. There are several key results here, both with regard to the regional mechanisms, and to the application of causal methods in marine biogeochemistry generally. The 18.6-year nodal variation in tidal mixing has a robust causal effect on the Oyashio O_2 time series (Figure 1c). Causal links from the tide can

https://doi.org/10.5194/egusphere-2026-5168
Preprint. Discussion started: 11 September 2026

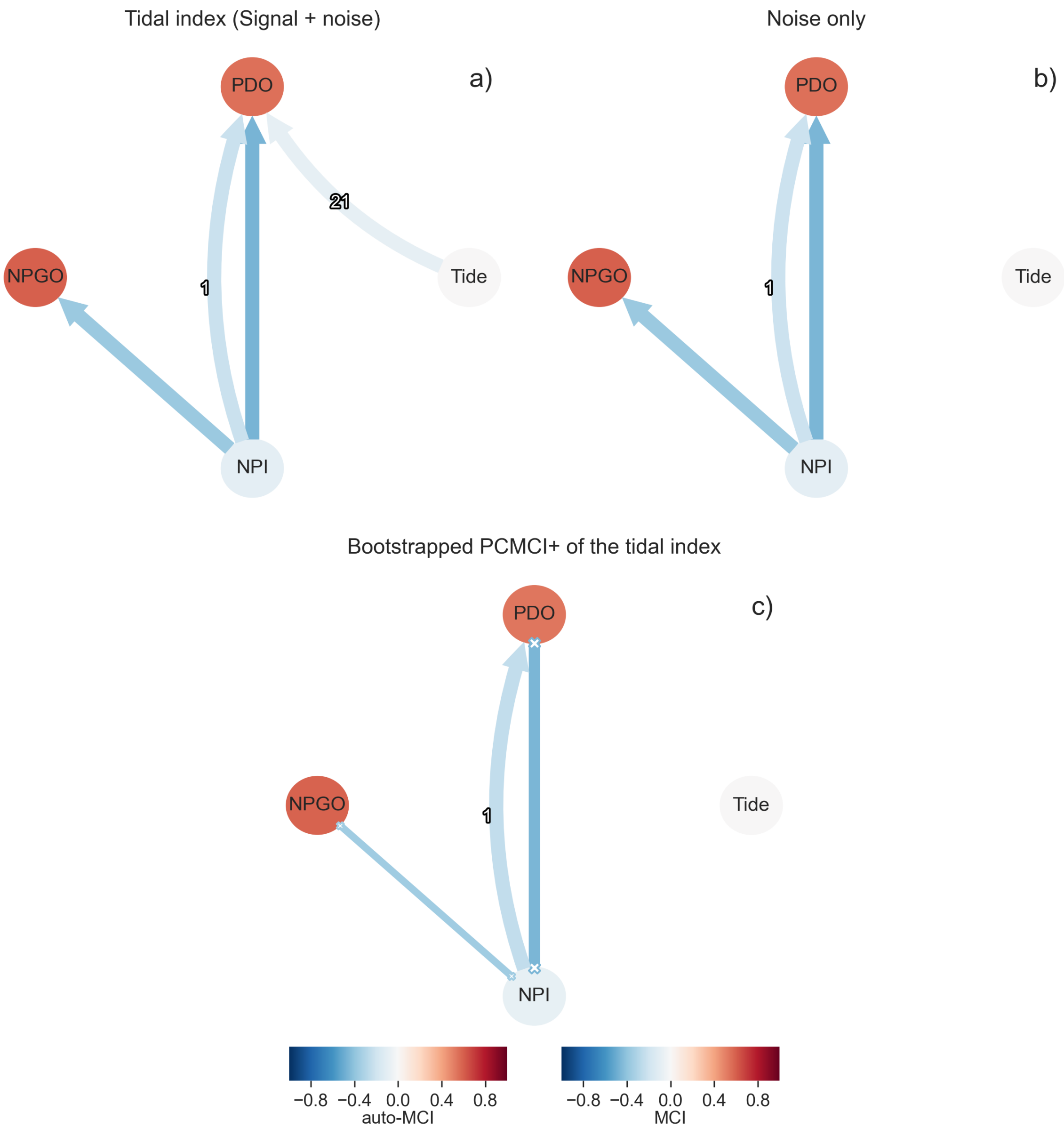

Figure 11. Graphs derived with PCMCI+ for the climate and tidal indices using their original monthly resolution, the time interval is now 1950 to 2022. PCMCI+ was applied to the dataset used in the Oyashio analysis **a)** and a version where the deterministic component of the index was removed **b)**. The robustness of these links was assessed with bootstrap-based , here the arrow thickness is proportional to that links occurrence rate, links ending in an **x** are unoriented causal links **c)**. Lag values are in units of months ($\tau = 1 = 1$ month). Arrows without numbers indicate an instantaneous effect within the data, an effect at $\tau = 0$. The "ocean" indices, the PDO and the NPGO, only respond to the "atmosphere" index, the NPI. While the tidal index is explicitly included, it is clearly not required.

https://doi.org/10.5194/egusphere-2026-5168
Preprint. Discussion started: 11 September 2026

also be identified within the AOU time series (Figures 7a), while there is a negligible tidal effect present in O_2^{sat} (Figure 8a). The tidal effect is not constant over density - a clear dependence on the density level exists, with the strength of the tidal effect maximised away from densities which commonly outcrop within the mixed layer (Mecking and Drushka, 2024). The lags of the tidal effects are quite long, up to 2 years for the maximum value, but they also demonstrate a density dependence. The lag values are consistent with estimates of the transport timescales between the outflows from the SO and the Oyashio region (Sasano et al., 2018). The O_2 dynamics are well explained with a linear tidal effect at the lag identified by PCMCI (Figure 10 and 9). Finally, we show that at seasonal resolution there are no causal effects encoded within the PDO, NPGO or NPI even though strong correlations are present in the data (Figure 5). These results highlight a useful attribute of PCMCI, but potentially many time series causal discovery methods; because it is designed to avoid irrelevant information (Section 2.2), we can greatly reduce the detection rate of false positive links, improving our ability to identify true causal relationships within the data. As Figure 5 illustrates, this should reduce a researcher's reliance on post-hoc justification of potentially spurious relationships.

We have also shown that it is easy to identify potentially spurious effects in the O_2 records of the North Pacific and miss key processes because of analytical choices, which we can demonstrate with existing work. Sasano et al. (2018) over a broad density range and presented a "two-layer" system to explain the deoxygenation and bi-decadal oscillations (their Figure 11), dividing at $\sim 26.8\sigma_\theta$. The upper layer is largely controlled by surface processes, and the lower by processes inside the SO. More recent work by Mecking and Drushka (2024) provides a complementary perspective; they quantified the downstream oxygenation effect of isopycnal outcropping in the North Pacific on to density surfaces $26.40\sigma_\theta$ to $26.80\sigma_\theta$, using the O_2 time series from the Ocean Station P in the North East Pacific. In contrast to Sasano et al. (2018) these results showed minimal, if any, influence of the nodal tide on the ventilation rate and O_2 content of this density range. The causal results here, help to reconcile these differing correlational models. While our identified causal effects qualitatively support Sasano et al. (2018), the process of conditioning out the auto-dependency of the O_2 arguably produces a better estimate of where the tidal effect occurs in density. However because Mecking and Drushka (2024) could only analyse outcropping isopycnals, non-outcropping processes ventilating the interior would always be missed. Despite this our results generally support the two-layer description from Sasano et al. (2018). We have shown that the tidal effect in the Oyashio region is restricted to density surfaces below the surface mixed layer; if a tidal effect exists closer to the surface it may be a mediated effect at short time scales (the tidal effect passes through a seasonal node, see Figure 12), which cannot be resolved in our analysis.

There are several limitations to our approach, beyond the key methodological assumptions that we make (Section 2.2). First, the causal link strength from the tidal index is still small; the causal link from the tidal index is the strongest identified on $27.10\sigma_\theta$, but still only explains $\sim$21% of the variance in the O_2 at that level (under the assumptions we make here, the squared MCI value gives a variance explained, as the partial correlation is conditional on the causal parents). Second, the linear effects assumed here appear to be defensible for multi-decadal O_2 time series, at a relatively coarse seasonal resolution. Yet it is not clear whether this assumption will continue to hold at higher temporal resolutions, but this would be an interesting question to pursue, perhaps using a numerical model to establish the kinds of causal discovery methods and conditional independence tests that would be appropriate for different sets of observations. Finally, the mechanism through which the nodal tidal signal enters in to the Oyashio O_2 record is actually unclear, and likely cannot be identified from this dataset as it currently exists. In

https://doi.org/10.5194/egusphere-2026-5168
Preprint. Discussion started: 11 September 2026

fact we cannot causally attribute the set of mechanisms generating the Oyashio deoxygenation from within this dataset (Figure 2). We can certainly use the existing literature and "domain knowledge" to highlight the tidal mixing in many locations along the Kuril island chain (Yagi and Yasuda, 2012; Yagi et al., 2014; Sasano et al., 2018; Mensah and Ohshima, 2021), and posit these locations as the origin of the bi-decadal signal. But this information is brought to the analysis *independent of the data*.

Considering where the tidal mixing occurs in the SO and possibly other regions such as the Bering sea (Andreev and Kusakabe, 2001), may matter for the predictions of future deoxygenation and decadal variability, as it will set the causal order of the system. With limited observations within the marginal sea, the effects of sea ice production and dense shelf water formation (DSW) in the north of the SO, the in-flows and tidal modification of WSAG water and the prolonged residence time in the Kuril basin are just some of the geographically specific processes that will determine the downstream O_2 (Figure 1a). Outside of the SO, recent work has demonstrated that the 18.6 year signal exists in the internal tide, indicating that the 18.6 year frequency could effect remote open ocean mixing processes as well, at least in principle (Zhao et al., 2026). Yet even limiting our focus to the marginal sea, the reason distinguishing between a general "nodal tidal effect" represented by a single index and mixing processes tied to specific locations, becomes apparent if we specify different causal models for Oyashio O_2 (Pearl, 2009b). Consider the following causal models (technically, directed acyclic graphs or "DAGs"), Figure 12. These qualitatively outline causal relationships which are *all* consistent with an exogenous tidal forcing causing the Oyashio O_2 oscillations.

These graphs (Figure 12) are not proposed as competing variants of the true or complete causal graph (which we do not know precisely), but as physically plausible examples which are compatible with the Tide $\rightarrow O_2$ effect found here. They are hypotheses, which imply different responses to interventions (Pearl, 2009b; Peters et al., 2017). A model where DSW mediates the tidal signal to the downstream O_2 predicts a different response to perturbations affecting DSW than one where the tidal effect reaches O_2 independently of DSW (ie. Figure 12, parallel pathways). Crucially, different causal models may be observationally equivalent, but imply different responses to interventions (Verma and Pearl, 2013). If the models in Figure 12 were interpreted as good representations of the real system, then they would imply quite different responses to perturbations such as the regions changing climate (Mensah and Ohshima, 2021; Mensah et al., 2024). For example, if a reduction in DSW formation preceded a reduction in O_2, that would be evidence towards the one of the DSW mediated models. Unfortunately, the limited data from within the sea limits the kinds of causal modelling we could perform - testing whether the O_2 record can be made independent of tidal mixing conditional on DSW would require observations of DSW, or if it remains unobserved, careful inclusion of its more easily observed causal parents, such as observations of the northern polynyas (Ohshima et al., 2014). These causal tools (Pearl, 2009b) could also support numerical modelling efforts. By designing simulations with a causal effect in mind (Tide $\rightarrow O_2$, Figure 12), a researcher could define the experiment more precisely, better discriminating between physical processes that might produce very similar observations, but differ in their response to interventions.

Finally, we have focused on the O_2 dynamics here, but a next step would be to consider the causal networks, effects and counterfactuals of the the wider ecosystem. In the Oyashio region, the ecosystem dynamics depend on limiting nutrients such as dissolved phosphate and iron (Nishioka et al., 2007), the concentration of phosphate appears to be undergoing a decline analogous to the deoxygenation (Ono et al., 2001; Yasunaka et al., 2016, 2021). Establishing a more complex causal model for the Oyashio region could allow counterfactual estimates of the region's marine biogeochemistry under different climate

https://doi.org/10.5194/egusphere-2026-5168
Preprint. Discussion started: 11 September 2026

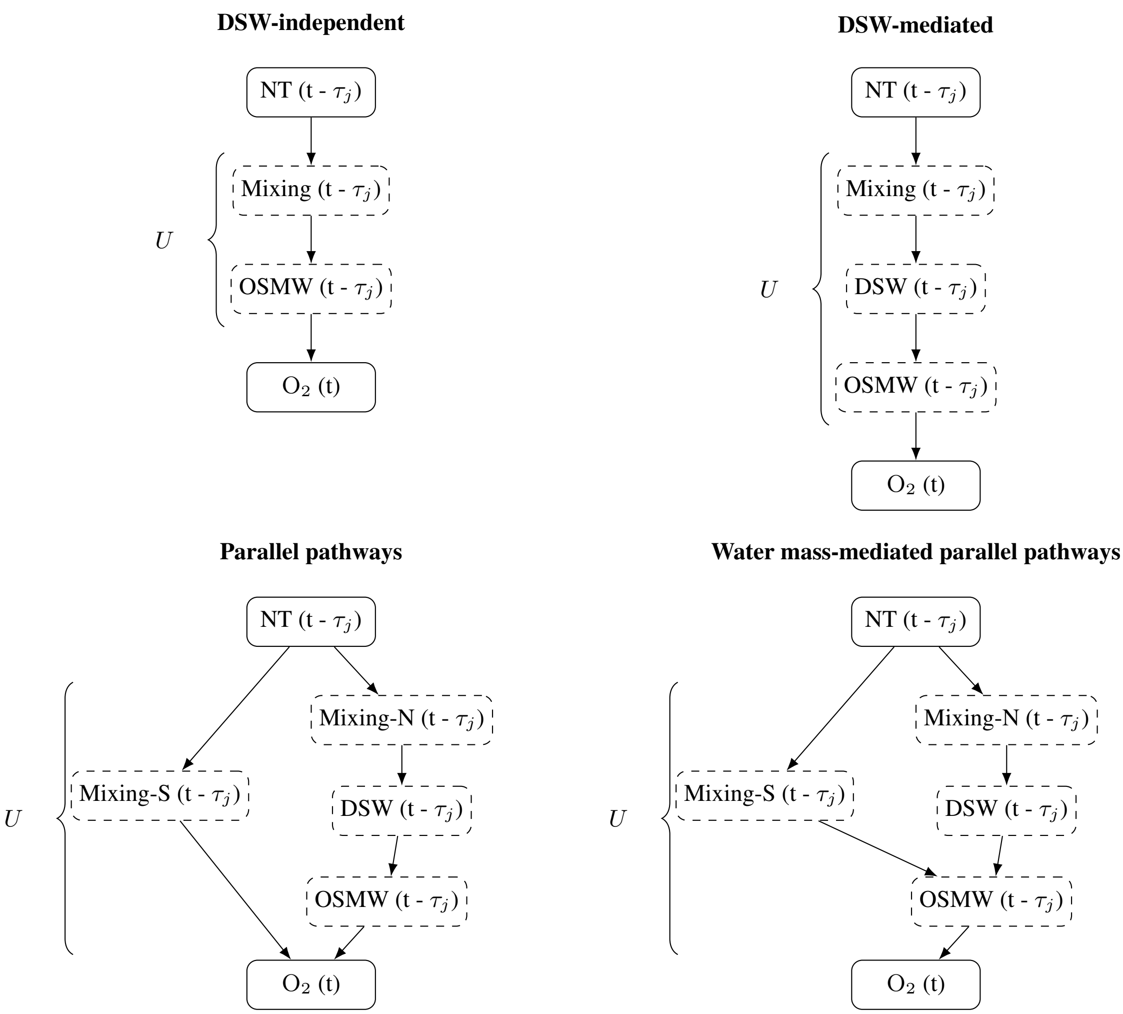

Figure 12. Plausible causal hypotheses that could produce the observed tide–O_2 relationship - other likely causes, which are assumed to be independent of tidal forcing such as the WSAG water, are omitted. Now rather than assuming we are representing tidal mixing explicitly, it is an unobserved process forced by the tide. Solid-bordered nodes are observed variables, whereas dashed-bordered nodes denote hypothesised intermediate latent processes in our analysis. The likely existence of lagged effects is indicated by $t - \tau_j$, of which there could be more than on. "Mixing" N/S (North/South) refers to the northern and southern ends of the Kuril island chain, ie. the Kruzenstern straits (North) and Bussol strait (South). The node U indicates the unobserved processes within the sea: but these do not need to be known to estimate the total tide $\rightarrow$ O_2 effect.

https://doi.org/10.5194/egusphere-2026-5168
Preprint. Discussion started: 11 September 2026

scenarios, or its response to perturbations (Hannart et al., 2016), while accounting for key processes such as the effect of tidal mixing. For example, a comparable dataset containing ecosystem and biogeochemical variables (ie. phosphate) and key physical indices such as the geostrophic transport through the region, could provide a data-based counterfactual model of possible ecosystem responses without parameterising remote tidal mixing in a numerical model, but while also consciously avoiding the construction of naive models optimised for prediction, rather than causal inference.

5 Conclusions

This analysis presents one of the first applications of a time series causal discovery method in the context of a historical oceanographic time series – where we have investigated the apparent relationship between the 18.6 nodal tidal cycle and the bi-decadal oscillations in O_2 in the Oyashio region. PCMCI identified robust causal links from the tidal index to O_2 time series, with the strongest links occurring at densities below the maximum reached by the late-winter mixed layer at a characteristic lag of $\sim$2 years. The corresponding causal relationship with AOU is opposite in sign over a similar density range, with much weaker evidence for a causal effect on to O_2^{sat}. Together, these results imply that the tidal influence on downstream O_2 is more closely associated with the oxygen history of interior water masses than with changes in the local O_2 solubility. Accounting for the temporal dependence of the O_2 time series substantially changes the interpretation of the previously observed tidal relationship. PCMCI identifies a much sparser set of links than lagged correlation, with a reduced link strength and removes much of the apparent lag structure associated with autocorrelation. We can show that a simplified causal model is nonetheless able to reproduce the observed lagged correlations. These results demonstrate the value of causal discovery for distinguishing persistent statistical associations from relationships that remain after accounting for the causal history of an oceanographic time series.

This analysis cannot identify the geographical location or complete physical pathway through which the tidal signal reaches the O_2 of the Oyashio region. The two-year lag is consistent with the residence time of OSMW in the Kuril basin, and the density distribution of the causal relationship is consistent with known regions of enhanced tidal mixing, particularly in the Bussol Strait. Nevertheless, several causal structures involving tidal modification of water masses, dense shelf-water formation and subsequent OSMW export could be compatible with the observations. These alternative causal models may make different predictions under interventions and therefore provide a framework for designing targeted observations and numerical experiments to distinguish between competing mechanisms. Finally we have provided some discussion of how causal discovery could complement mechanistic ocean modelling, by providing observational constraints on which relationships require physical explanation, while explicitly highlighting any remaining uncertainty in the causal structure. Extending this approach to observations of nutrients, ecosystem variables, transport and water-mass formation could provide a basis for constructing more complete causal models of regional marine biogeochemistry and for evaluating counterfactual responses to the regions changing climate.

https://doi.org/10.5194/egusphere-2026-5168
Preprint. Discussion started: 11 September 2026

Code and data availability. The archived code to perform this analysis can be found at [zenodo archive], including the preprocessing procedure and the version of Tigramite used at the time. The workflow should be compatible with recent versions of Tigramite. The original data can also be found at: github.com/BWBlack/oyashio_causal_discovery

Appendix A

Author contributions. BB conceived of the original study under the supervision of OA and RB. The analysis was performed by BB, the manuscript was written by BB with contributions from all authors.

Competing interests. The authors have no competing interests.

Acknowledgements. BB would like to highlight the support of the GW4+ doctoral training program and the support of the University of Bristol, School of Geographical Sciences as well as the continued support of the Simons Foundation Grants LS-CBIOMES-00827829 and LS-CBIOMES-01157243. BB would like to thank Daisuke Sasano for providing access to the preprocessed time series from the Oyashio region and Sam Ditkovsky for the helpful comments on the manuscript. UN contributed to this work while affiliated with Technische Universität Berlin.

https://doi.org/10.5194/egusphere-2026-5168
Preprint. Discussion started: 11 September 2026

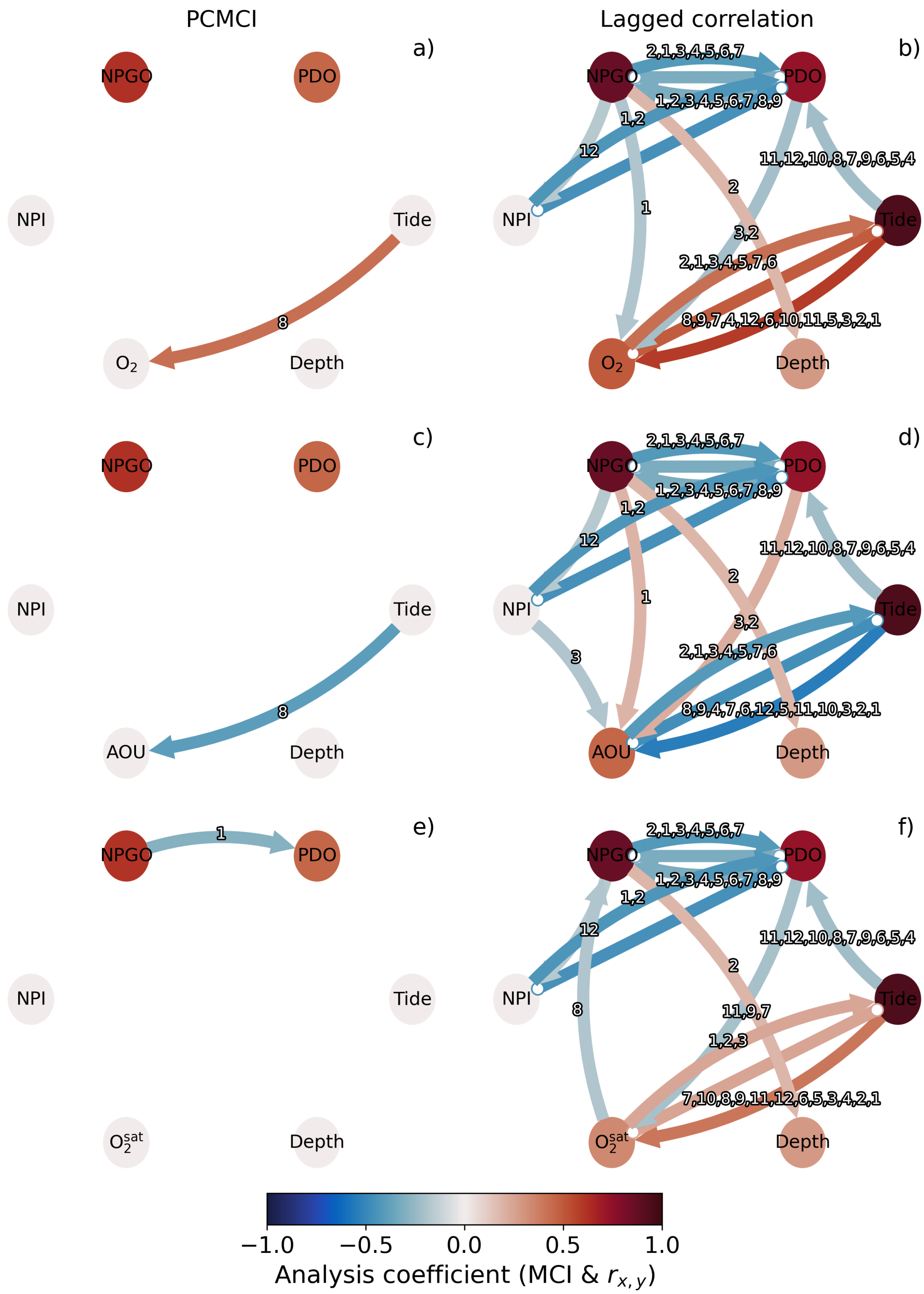

Figure A1. Causal (**a, b, c**) and correlational (**d, e, f**) graphs for dissolved oxygen (**a**, **b**, O_2), apparent oxygen utilisation (**c**, **d**, AOU) and the solubility of oxygen (**e**, **f**, O_2^{sat}). Node and arrow colours indicate the maximum of the mutual conditional information value (MCI) or lagged-correlation coefficient. The numbers on the arrows are lags in units of seasons, ordered according to the value of the coefficient (causal or correlational) - largest first.

https://doi.org/10.5194/egusphere-2026-5168
Preprint. Discussion started: 11 September 2026

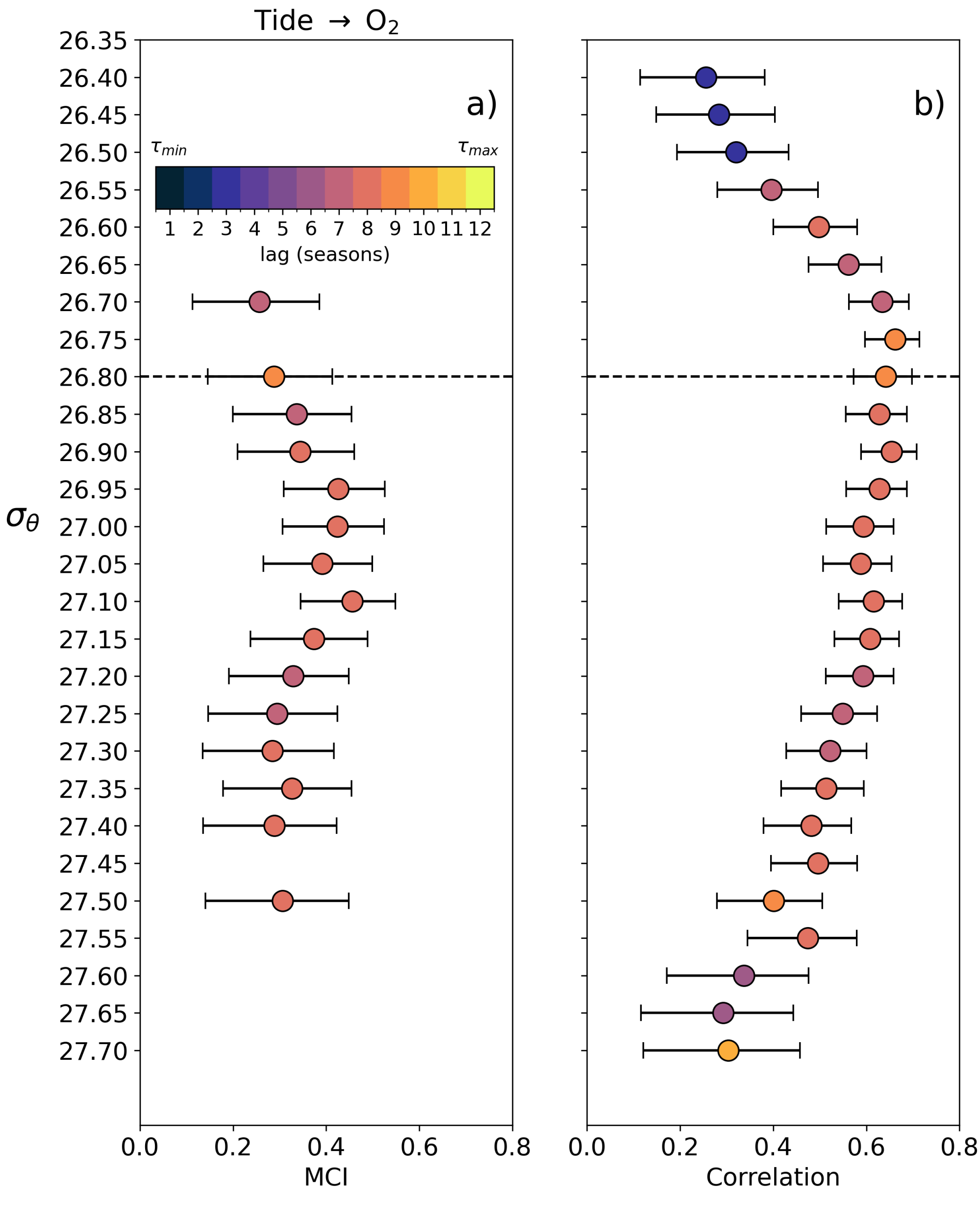

Figure A2. A sensitivity test to a change in α when analysing the dissolved Oxygen (O_2) time series, the $\alpha = 0.05$. The distribution over density of **a)** causal links from the nodal tidal index to the O_2 time series, **b)** the lagged correlation coefficient. In both a) and b) error bars indicate the 95% confidence interval. The lag magnitude (τ), is given by the colour scale in units of seasons. The dashed line indicates the approximate maximum density reached by the late-winter mixed layer.

https://doi.org/10.5194/egusphere-2026-5168
Preprint. Discussion started: 11 September 2026

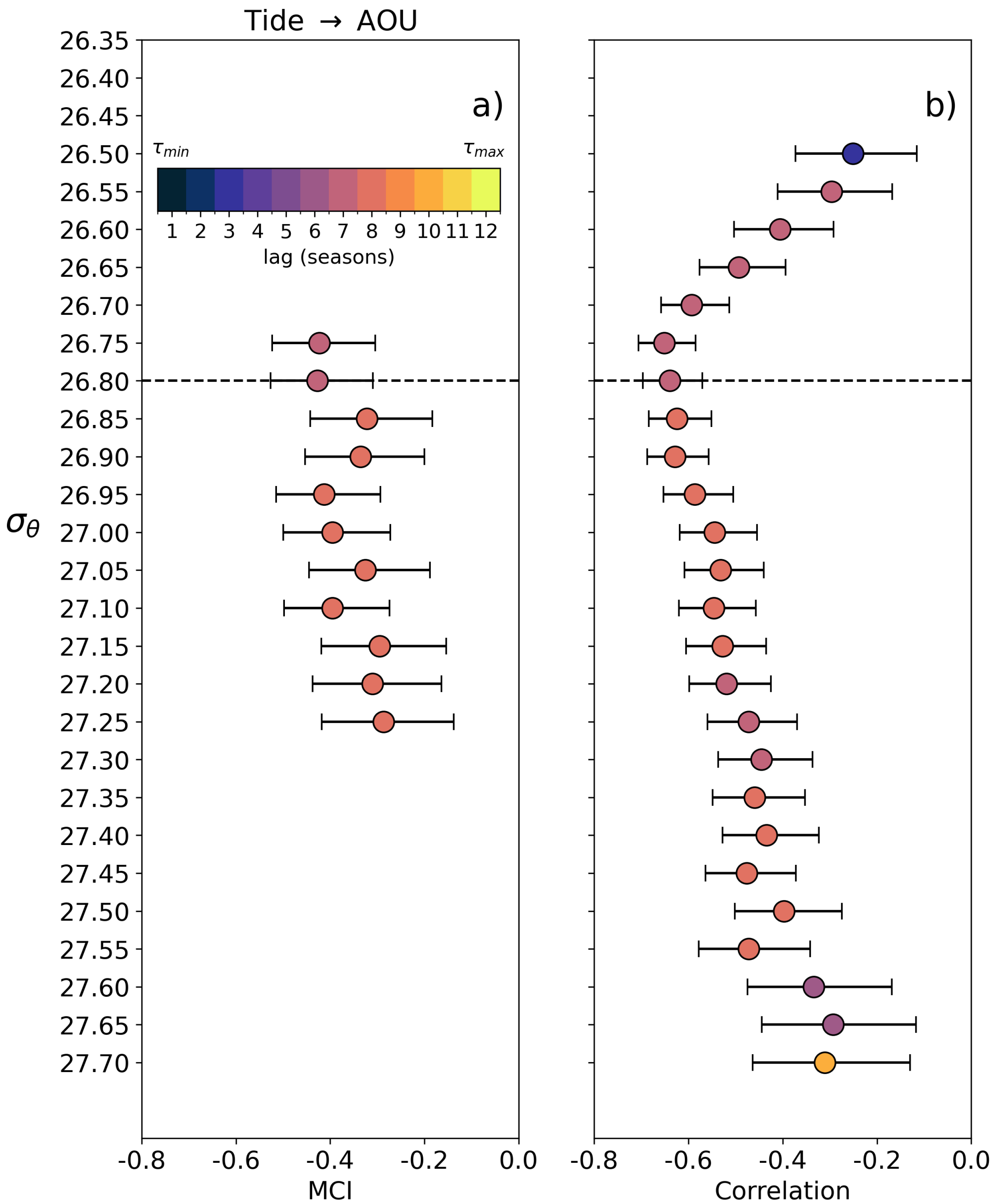

Figure A3. A sensitivity test to a change in α when analysing the apparent oxygen utilisation (AOU) time series, the $\alpha = 0.05$. The distribution over density of **a)** causal links from the nodal tidal index to the AOU time series, **b)** the lagged correlation coefficient. The lag magnitude (τ), is given by the colour scale in units of seasons. The dashed line indicates the approximate maximum density reached by the late-winter mixed layer.

https://doi.org/10.5194/egusphere-2026-5168
Preprint. Discussion started: 11 September 2026

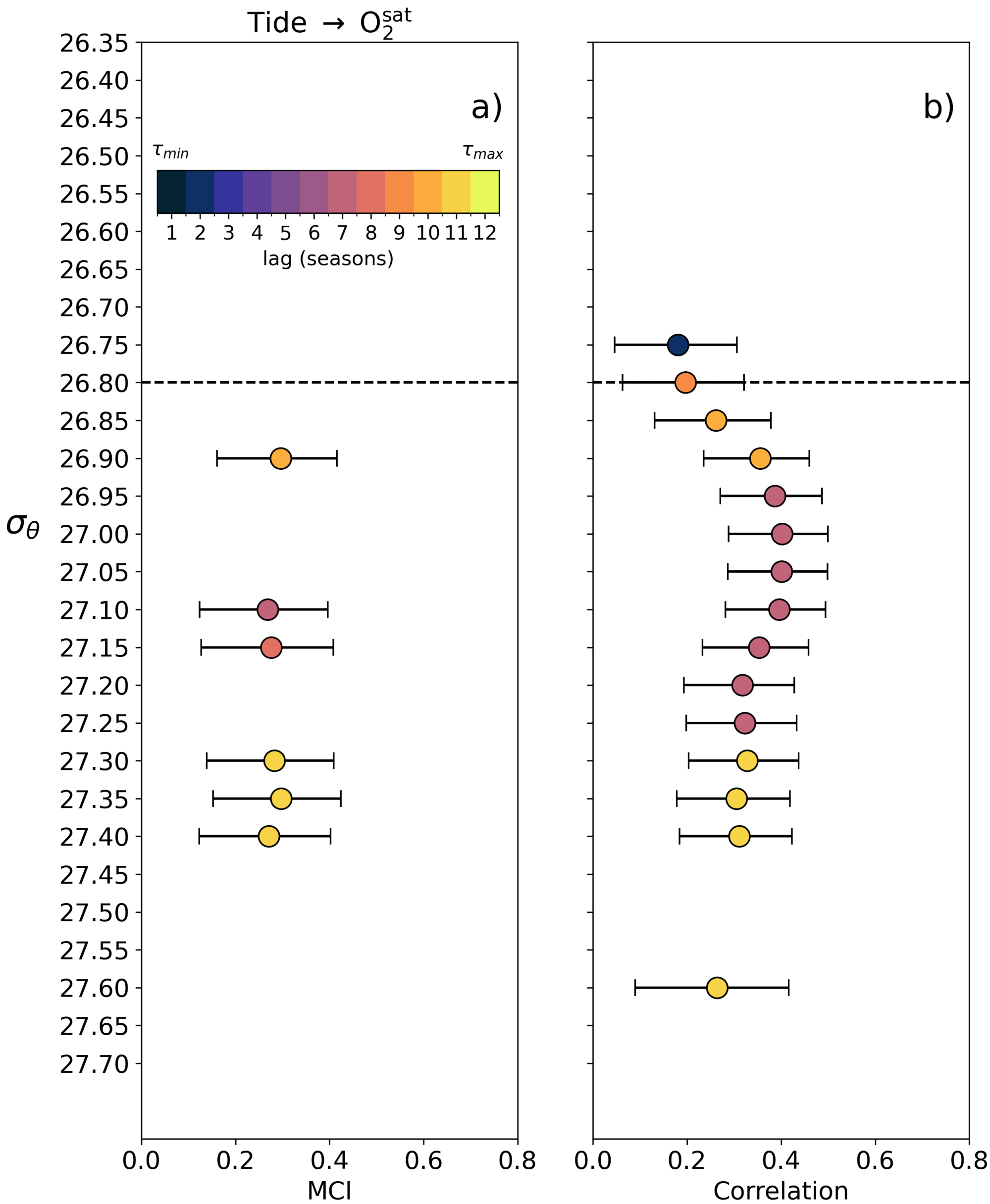

Figure A4. A sensitivity test to a change in α when analysing the Oxygen solubility (O_2^{sat}) time series, the $\alpha = 0.05$. The distribution over density of **a)** causal links from the nodal tidal index to the O_2^{sat} time series, **b)** the lagged correlation coefficient. The lag magnitude (τ), is given by the colour scale in units of seasons. The dashed line indicates the approximate maximum density reached by the late-winter mixed layer.

https://doi.org/10.5194/egusphere-2026-5168
Preprint. Discussion started: 11 September 2026

References

Abecasis, D., Fragkopoulou, E., Claro, B., and Assis, J.: Biophysical modelling and graph theory identify key connectivity hubs in the Mediterranean marine reserve network, Frontiers in Marine Science, 9, 1000 687, 2023.

Akima, H.: A method of univariate interpolation that has the accuracy of a third-degree polynomial, ACM Transactions on Mathematical Software (TOMS), 17, 341–366, 1991.

Andreev, A. G. and Kusakabe, M.: Interdecadal variability in dissolved oxygen in the intermediate water layer of the Western Subarctic Gyre and Kuril Basin (Okhotsk Sea), Geophysical Research Letters, 28, 2453–2456, https://doi.org/https://doi-org.bris.idm.oclc.org/10.1029/2000GL012688, 2001.

Andrews, O., Bindoff, N., Halloran, P., Ilyina, T., and Le Quéré, C.: Detecting an external influence on recent changes in oceanic oxygen using an optimal fingerprinting method, Biogeosciences, 10, 1799–1813, 2013.

Bahl, A., Gnanadesikan, A., and Pradal, M.-A.: Variations in ocean deoxygenation across earth system models: isolating the role of parameterized lateral mixing, Global Biogeochemical Cycles, 33, 703–724, 2019.

Bénard, G., Gehlen, M., and Vrac, M.: Evolution of causal relationships under climate change: controls of Net Primary Productivity in the North Altantic Subpolar Gyre, EGUsphere, 2025, 1–23, 2025a.

Bénard, G., Gehlen, M., and Vrac, M.: A causality-based method for multi-model comparison: application to relationships between atmospheric, oceanic and marine biogeochemical variables, Earth System Dynamics, 16, 1085–1102, 2025b.

Benjamini, Y. and Hochberg, Y.: Controlling the false discovery rate: a practical and powerful approach to multiple testing, Journal of the Royal statistical society: series B (Methodological), 57, 289–300, 1995.

Broecker, W. S.: “NO”, a conservative water-mass tracer, Earth and Planetary Science Letters, 23, 100–107, 1974.

Caldwell, P., Merrifield, M., and Thompson, P.: Sea level measured by tide gauges from global oceans—The Joint Archive for sea level holdings, version 5.5. NOAA/National Centers for Environmental Information, 2015.

Camps-Valls, G., Gerhardus, A., Ninad, U., Varando, G., Martius, G., Balaguer-Ballester, E., Vinuesa, R., Diaz, E., Zanna, L., and Runge, J.: Discovering causal relations and equations from data, Physics Reports, 1044, 1–68, 2023.

Carpenter, J. H.: The Chesapeake Bay Institute technique for the Winkler dissolved oxygen method, Limnology and Oceanography, 10, 141–143, 1965.

Codiga, D. L.: Unified tidal analysis and prediction using the UTide Matlab functions, 2011.

Colombo, D., Maathuis, M. H., et al.: Order-independent constraint-based causal structure learning., J. Mach. Learn. Res., 15, 3741–3782, 2014.

Damien, P., Molemaker, J., McCoy, D., Dollery, D., Guiet, J., Bianchi, D., and McWilliams, J. C.: Development of a Mesoscale- and Tide-Resolving Ocean–Biogeochemistry Model for the Pacific: Tidal Enhancement of the Biological Carbon Pump, Journal of Advances in Modeling Earth Systems, 18, e2025MS005 458, https://doi.org/https://doi.org/10.1029/2025MS005458, 2026.

Debeire, K., Gerhardus, A., Runge, J., and Eyring, V.: Bootstrap aggregation and confidence measures to improve time series causal discovery, in: Causal Learning and Reasoning, pp. 979–1007, PMLR, 2024.

Deutsch, C., Berelson, W., Thunell, R., Weber, T., Tems, C., McManus, J., Crusius, J., Ito, T., Baumgartner, T., Ferreira, V., et al.: Centennial changes in North Pacific anoxia linked to tropical trade winds, Science, 345, 665–668, 2014.

Di Lorenzo, E., Schneider, N., Cobb, K. M., Franks, P., Chhak, K., Miller, A. J., McWilliams, J. C., Bograd, S. J., Arango, H., Curchitser, E., et al.: North Pacific Gyre Oscillation links ocean climate and ecosystem change, Geophysical research letters, 35, 2008.

https://doi.org/10.5194/egusphere-2026-5168
Preprint. Discussion started: 11 September 2026

Ditkovsky, S. J. and Resplandy, L.: Tides Boost Primary Production in the Indian Ocean, Global Biogeochemical Cycles, 39, e2025GB008 596, https://doi.org/https://doi.org/10.1029/2025GB008596, 2025.

Duprey, N., Foreman, A., Carriquiry, J., Charles, C., Sanchez, S., Vonhof, H., Rubach, F., Rabenstein, R., Rohr, M., Reyes-Bonilla, H., et al.: Decadal oscillations in the ocean's largest oxygen-deficient zone, Science, 386, 1019–1024, 2024.

Ebert-Uphoff, I. and Deng, Y.: Causal discovery for climate research using graphical models, Journal of Climate, 25, 5648–5665, 2012.

Emile-Geay, J., Cane, M. A., Naik, N., Seager, R., Clement, A. C., and van Geen, A.: Warren revisited: Atmospheric freshwater fluxes and "Why is no deep water formed in the North Pacific", Journal of Geophysical Research: Oceans, 108, https://doi.org/https://doi-org.bris.idm.oclc.org/10.1029/2001JC001058, 2003.

Flato, G. M.: Earth system models: an overview, Wiley Interdisciplinary Reviews: Climate Change, 2, 783–800, 2011.

Fukamachi, Y., Mizuta, G., Ohshima, K. I., Talley, L. D., Riser, S. C., and Wakatsuchi, M.: Transport and modification processes of dense shelf water revealed by long-term moorings off Sakhalin in the Sea of Okhotsk, Journal of Geophysical Research: Oceans, 109, https://doi.org/https://doi.org/10.1029/2003JC001906, 2004.

Garcia, H. E. and Gordon, L. I.: Oxygen solubility in seawater: Better fitting equations, Limnology and Oceanography, 37, 1307–1312, https://doi.org/10.4319/lo.1992.37.6.1307, 1992.

Garrett, C.: Mixing in the ocean interior, Dynamics of Atmospheres and Oceans, 3, 239–265, 1979.

Garrett, C.: Internal tides and ocean mixing, Science, 301, 1858–1859, 2003.

Gladyshev, S., Talley, L., Kantakov, G., Khen, G., and Wakatsuchi, M.: Distribution, formation, and seasonal variability of Okhotsk Sea Mode Water, Journal of Geophysical Research: Oceans, 108, 2003.

Gnanadesikan, A., Dunne, J., and John, J.: Understanding why the volume of suboxic waters does not increase over centuries of global warming in an Earth System Model, Biogeosciences, 9, 1159–1172, 2012.

Griffith, G. P.: Closing the gap between causality, prediction, emergence, and applied marine management, ICES Journal of Marine Science, 77, 1456–1462, 2020.

Hannart, A. and Naveau, P.: Probabilities of causation of climate changes, Journal of Climate, 31, 5507–5524, 2018.

Hannart, A., Pearl, J., Otto, F., Naveau, P., and Ghil, M.: Causal counterfactual theory for the attribution of weather and climate-related events, Bulletin of the American Meteorological Society, 97, 99–110, 2016.

Hayduk, L., Cummings, G., Stratkotter, R., Nimmo, M., Grygoryev, K., Dosman, D., Gillespie, M., Pazderka-Robinson, H., and Boadu, K.: Pearl's D-separation: One more step into causal thinking, Structural Equation Modeling, 10, 289–311, 2003.

Ito, T., Minobe, S., Long, M. C., and Deutsch, C.: Upper ocean O2 trends: 1958–2015, Geophysical Research Letters, 44, 4214–4223, 2017.

Ito, T., Long, M. C., Deutsch, C., Minobe, S., and Sun, D.: Mechanisms of low-frequency oxygen variability in the North Pacific, Global Biogeochemical Cycles, 33, 110–124, 2019.

Joshi, M., Hall, R. A., Stevens, D. P., and Hawkins, E.: The modelled climatic response to the 18.6-year lunar nodal cycle and its role in decadal temperature trends, Earth System Dynamics, 14, 443–455, 2023.

Jutras, M., Bushinsky, S. M., Cerovečki, I., and Briggs, N.: Mixing Accounts for More Than Half of Biogeochemical Changes Along Mode Water Ventilation Pathways, Geophysical Research Letters, 52, e2024GL113 789, https://doi.org/https://doi.org/10.1029/2024GL113789, 2025.

Keeling, C. D. and Whorf, T. P.: Possible forcing of global temperature by the oceanic tides, Proceedings of the National Academy of Sciences, 94, 8321–8328, 1997.

Keeling, C. D. and Whorf, T. P.: The 1,800-year oceanic tidal cycle: A possible cause of rapid climate change, Proceedings of the National Academy of Sciences, 97, 3814–3819, 2000.

Keeling, R. F., Körtzinger, A., and Gruber, N.: Ocean deoxygenation in a warming world, Annual review of marine science, 2, 199–229, 2010.

Kitani, K.: An oceanographic study of the Okhotsk Sea-particularly in regard to cold waters, Bull. Far. Seas. Fish. Res., 9, 45–77, 1973.

Kretschmer, M., Coumou, D., Donges, J. F., and Runge, J.: Using causal effect networks to analyze different Arctic drivers of midlatitude winter circulation, Journal of climate, 29, 4069–4081, 2016.

Kretschmer, M., Adams, S. V., Arribas, A., Prudden, R., Robinson, N., Saggioro, E., and Shepherd, T. G.: Quantifying causal pathways of teleconnections, Bulletin of the American Meteorological Society, 102, E2247–E2263, 2021.

Krich, C., Runge, J., Miralles, D. G., Migliavacca, M., Perez-Priego, O., El-Madany, T., Carrara, A., and Mahecha, M. D.: Estimating causal networks in biosphere–atmosphere interaction with the PCMCI approach, Biogeosciences, 17, 1033–1061, 2020.

Kumar, P., Kuttippurath, J., and Mitra, A.: Causal discovery of drivers of surface ozone variability in Antarctica using a deep learning algorithm, Environmental science: Processes & impacts, 24, 447–459, 2022.

Lévy, M., Resplandy, L., Palter, J. B., Couespel, D., and Lachkar, Z.: The crucial contribution of mixing to present and future ocean oxygen distribution, in: Ocean mixing, pp. 329–344, Elsevier, 2022.

Loder, J. W. and Garrett, C.: The 18.6-year cycle of sea surface temperature in shallow seas due to variations in tidal mixing, Journal of Geophysical Research: Oceans, 83, 1967–1970, 1978.

Long, M. C., Deutsch, C., and Ito, T.: Finding forced trends in oceanic oxygen, Global Biogeochemical Cycles, 30, 381–397, 2016.

Mantua, N. J. and Hare, S. R.: The Pacific decadal oscillation, Journal of oceanography, 58, 35–44, 2002.

Mecking, S. and Drushka, K.: Linking northeastern North Pacific oxygen changes to upstream surface outcrop variations, Biogeosciences, 21, 1117–1133, 2024.

Mecking, S., Langdon, C., Feely, R. A., Sabine, C. L., Deutsch, C. A., and Min, D.-H.: Climate variability in the North Pacific thermocline diagnosed from oxygen measurements: An update based on the US CLIVAR/CO2 Repeat Hydrography cruises, Global Biogeochemical Cycles, 22, 2008.

Mensah, V. and Ohshima, K. I.: Weakened overturning and tide control the properties of Oyashio Intermediate Water, a key water mass in the North Pacific, Scientific reports, 11, 14 526, 2021.

Mensah, V., Ohshima, K. I., Drucker, R., and Riser, S.: Evaluation of the Water Mass Composition in the Sea of Okhotsk and Its Long-Term Change Using an Advanced Mapping Technique, Journal of Geophysical Research: Oceans, 129, e2023JC020 374, https://doi.org/https://doi.org/10.1029/2023JC020374, 2024.

Munk, W., Dzieciuch, M., and Jayne, S.: Millennial climate variability: Is there a tidal connection?, Journal of climate, 15, 370–385, 2002.

Nakamura, T., Toyoda, T., Ishikawa, Y., and Awaji, T.: Enhanced ventilation in the Okhotsk Sea through tidal mixing at the Kuril Straits, Deep Sea Research Part I: Oceanographic Research Papers, 53, 425–448, 2006.

Navarra, G. G., Deutsch, C., and Mazloff, M.: Causal drivers of Southern Ocean greening in the Antarctic Circumpolar Current, 2026.

Nishioka, J., Ono, T., Saito, H., Nakatsuka, T., Takeda, S., Yoshimura, T., Suzuki, K., Kuma, K., Nakabayashi, S., Tsumune, D., et al.: Iron supply to the western subarctic Pacific: Importance of iron export from the Sea of Okhotsk, Journal of Geophysical Research: Oceans, 112, 2007.

Ohshima, K. I., Nakanowatari, T., Riser, S., and Wakatsuchi, M.: Seasonal variation in the in-and outflow of the Okhotsk Sea with the North Pacific, Deep Sea Research Part II: Topical Studies in Oceanography, 57, 1247–1256, 2010.

https://doi.org/10.5194/egusphere-2026-5168
Preprint. Discussion started: 11 September 2026

Ohshima, K. I., Nakanowatari, T., Riser, S., Volkov, Y., and Wakatsuchi, M.: Freshening and dense shelf water reduction in the Okhotsk Sea linked with sea ice decline, Progress in Oceanography, 126, 71–79, 2014.

Ono, J., Ohshima, K. I., Mizuta, G., Fukamachi, Y., and Wakatsuchi, M.: Amplification of diurnal tides over Kashevarov Bank in the Sea of Okhotsk and its impact on water mixing and sea ice, Deep Sea Research Part I: Oceanographic Research Papers, 53, 409–424, 2006.

Ono, T., Midorikawa, T., Watanabe, Y., Tadokoro, K., and Saino, T.: Temporal increases of phosphate and apparent oxygen utilization in the subsurface waters of western subarctic Pacific from 1968 to 1998, Geophysical Research Letters, 28, 3285–3288, 2001.

Osafune, S. and Yasuda, I.: Bidecadal variability in the intermediate waters of the northwestern subarctic Pacific and the Okhotsk Sea in relation to 18.6-year period nodal tidal cycle, Journal of Geophysical Research: Oceans, 111, 2006.

Osafune, S. and Yasuda, I.: Remote impacts of the 18.6 year period modulation of localized tidal mixing in the North Pacific, Journal of Geophysical Research: Oceans, 118, 3128–3137, 2013.

Oschlies, A., Brandt, P., Stramma, L., and Schmidtko, S.: Drivers and mechanisms of ocean deoxygenation, Nature Geoscience, 11, 467–473, 2018.

Palter, J. B. and Trossman, D. S.: The sensitivity of future ocean oxygen to changes in ocean circulation, Global Biogeochemical Cycles, 32, 738–751, 2018.

Pearl, J.: Causality : Models, Reasoning and Inference, Cambridge University Press, 2nd edn., 2009a.

Pearl, J.: Causality, Cambridge University Press, 2009b.

Peters, J., Janzing, D., and Schölkopf, B.: Elements of causal inference: foundations and learning algorithms, The MIT press, 2017.

Portela, E., Kolodziejczyk, N., Vic, C., and Thierry, V.: Physical Mechanisms Driving Oxygen Subduction in the Global Ocean, Geophysical Research Letters, 47, 2020.

Pugh, D.: Sea-Level Science: Understanding Tides, Surges, Tsunamis and Mean Sea-Level Changes, vol. 407, Cambridge University Press, 2014.

Ray, R. D.: Decadal climate variability: Is there a tidal connection?, Journal of Climate, 20, 3542–3560, 2007.

Rippeth, T. P.: Mixing in seasonally stratified shelf seas: A shifting paradigm, Philosophical Transactions of the Royal Society A: Mathematical, Physical and Engineering Sciences, 363, 2837–2854, 2005.

Rohr, T., Richardson, A. J., Lenton, A., Chamberlain, M. A., and Shadwick, E. H.: Zooplankton grazing is the largest source of uncertainty for marine carbon cycling in CMIP6 models, Communications Earth & Environment, 4, 212, 2023.

Runge, J.: Discovering contemporaneous and lagged causal relations in autocorrelated nonlinear time series datasets, in: Conference on Uncertainty in Artificial Intelligence, pp. 1388–1397, Pmlr, 2020.

Runge, J., Petoukhov, V., and Kurths, J.: Quantifying the strength and delay of climatic interactions: The ambiguities of cross correlation and a novel measure based on graphical models, Journal of climate, 27, 720–739, 2014.

Runge, J., Petoukhov, V., Donges, J. F., Hlinka, J., Jajcay, N., Vejmelka, M., Hartman, D., Marwan, N., Paluš, M., and Kurths, J.: Identifying causal gateways and mediators in complex spatio-temporal systems, Nature communications, 6, 8502, 2015.

Runge, J., Bathiany, S., Bollt, E., Camps-Valls, G., Coumou, D., Deyle, E., Glymour, C., Kretschmer, M., Mahecha, M. D., Muñoz-Marí, J., et al.: Inferring causation from time series in Earth system sciences, Nature communications, 10, 2553, 2019a.

Runge, J., Nowack, P., Kretschmer, M., Flaxman, S., and Sejdinovic, D.: Detecting and quantifying causal associations in large nonlinear time series datasets, Science advances, 5, eaau4996, 2019b.

Sasano, D., Takatani, Y., Kosugi, N., Nakano, T., Midorikawa, T., and Ishii, M.: Multidecadal trends of oxygen and their controlling factors in the western North Pacific, Global Biogeochemical Cycles, 29, 935–956, 2015.

Sasano, D., Takatani, Y., Kosugi, N., Nakano, T., Midorikawa, T., and Ishii, M.: Decline and Bidecadal Oscillations of Dissolved Oxygen in the Oyashio Region and Their Propagation to the Western North Pacific, Global Biogeochemical Cycles, 32, 909–931, 2018.

Saunders, M. I., Brown, C. J., Foley, M. M., Febria, C. M., Albright, R., Mehling, M. G., Kavanaugh, M. T., and Burfeind, D. D.: Human impacts on connectivity in marine and freshwater ecosystems assessed using graph theory: a review, Marine and Freshwater Research, 67, 277–290, 2015.

Schmidtko, S., Stramma, L., and Visbeck, M.: Decline in global oceanic oxygen content during the past five decades, Nature, 542, 335–339, https://doi.org/10.1038/nature21399, 2017.

Shcherbina, A. Y., Talley, L. D., and Rudnick, D. L.: Dense water formation on the northwestern shelf of the Okhotsk Sea: 1. Direct observations of brine rejection, Journal of Geophysical Research: Oceans, 109, https://doi.org/https://doi.org/10.1029/2003JC002196, 2004a.

Simpson, J. H., Crawford, W. R., Rippeth, T. P., Campbell, A. R., and Cheok, J. V.: The vertical structure of turbulent dissipation in shelf seas, Journal of Physical Oceanography, 26, 1579–1590, 1996.

Spirtes, P., Glymour, C., and Scheines, R.: Causation, prediction, and search, MIT press, 2001.

Stramma, L. and Schmidtko, S.: Global evidence of ocean deoxygenation, IUCN, 2019.

Stramma, L., Schmidtko, S., Bograd, S. J., Ono, T., Ross, T., Sasano, D., and Whitney, F. A.: Trends and decadal oscillations of oxygen and nutrients at 50 to 300 m depth in the equatorial and North Pacific, Biogeosciences, 17, 813–831, 2020.

Takatani, Y., Sasano, D., Nakano, T., Midorikawa, T., and Ishii, M.: Decrease of dissolved oxygen after the mid-1980s in the western North Pacific subtropical gyre along the 137° E repeat section, Global Biogeochemical Cycles, 26, 2012.

Takizawa, T.: Characteristics of the Soya warm current in the Okhotsk Sea, Journal of the Oceanographical Society of Japan, 38, 281–292, 1982.

Talley, L. D.: Distribution and formation of North Pacific intermediate water, Journal of Physical Oceanography, 23, 517–537, 1993.

Treml, E. A., Halpin, P. N., Urban, D. L., and Pratson, L. F.: Modeling population connectivity by ocean currents, a graph-theoretic approach for marine conservation, Landscape Ecology, 23, 19–36, 2008.

Trenberth, K. E. and Hurrell, J. W.: Decadal atmosphere-ocean variations in the Pacific, Climate Dynamics, 9, 303–319, 1994.

Verma, T. S. and Pearl, J.: On the equivalence of causal models, arXiv preprint arXiv:1304.1108, 2013.

Wahl, J., Ninad, U., and Runge, J.: Vector causal inference between two groups of variables, in: Proceedings of the AAAI Conference on Artificial Intelligence, vol. 37, pp. 12 305–12 312, 2023.

Warren, B. A.: Why is no deep water formed in the North Pacific?, Journal of Marine Research, 41, 327–347, 1983.

Watanabe, Y. W., Wakita, M., Maeda, N., Ono, T., and Gamo, T.: Synchronous bidecadal periodic changes of oxygen, phosphate and temperature between the Japan Sea deep water and the North Pacific intermediate water, Geophysical research letters, 30, 2003.

Whitney, F. A., Freeland, H. J., and Robert, M.: Persistently declining oxygen levels in the interior waters of the eastern subarctic Pacific, Progress in Oceanography, 75, 179–199, 2007.

Woodworth, P. L.: A note on the nodal tide in sea level, Journal of Coastal Research, 28, 316–323, 2012.

Yagi, M. and Yasuda, I.: Deep intense vertical mixing in the Bussol'Strait, Geophysical Research Letters, 39, 2012.

Yagi, M., Yasuda, I., Tanaka, T., Tanaka, Y., Ono, K., Ohshima, K. I., and Katsumata, K.: Re-evaluation of turbulent mixing vertical structure in the Bussol'Strait and its impact on water masses in the Okhotsk Sea and the North Pacific, Progress in Oceanography, 126, 121–134, 2014.

https://doi.org/10.5194/egusphere-2026-5168
Preprint. Discussion started: 11 September 2026

Yasuda, I., Osafune, S., and Tatebe, H.: Possible explanation linking 18.6-year period nodal tidal cycle with bi-decadal variations of ocean and climate in the North Pacific, Geophysical research letters, 33, 2006.

Yasunaka, S., Ono, T., Nojiri, Y., Whitney, F., Wada, C., Murata, A., Nakaoka, S., and Hosoda, S.: Long-term variability of surface nutrient concentrations in the North Pacific, Geophysical Research Letters, 43, 3389–3397, 2016.

Yasunaka, S., Mitsudera, H., Whitney, F., and Nakaoka, S.-i.: Nutrient and dissolved inorganic carbon variability in the North Pacific, Journal of oceanography, 77, 3–16, 2021.

Zhao, Z., Ji, C., Green, M., and Ray, R.: The 18.6-year Lunar Nodal Cycle in Internal Tides, https://doi.org/10.13140/RG.2.2.31876.28803, 2026.